

# **BOREHOLE GEOLOGY AND DISTRIBUTION OF ALTERATION MINERALOGY IN OW 927B IN OLKARIA GEOTHERMAL FIELD, KENYA**

**Monicah Kimonda Kibet**

Kenya Electricity Generating Company PLC

P.O. Box 785-20117

Naivasha

KENYA

*monicah\_kibet@yahoo.com*

## **ABSTRACT**

Well OW 927B was drilled in Olkaria Domes geothermal field for gathering steam for the Olkaria IV power plant. The lithology of OW 927B is typical for the Olkaria geothermal field. At the top are the Olkaria volcanics, which comprise of pyroclastics, comendites and rhyolites underlain by Olkaria basalts (basalt with intercalation of breccia, tuff, trachyte), which act as the cap rock. The oldest formations are the plateau trachytes (trachyte, intercalation of tuff, basalt, and intrusion), which is the reservoir rock. The basalts are somewhat deeper here than in other parts of the Olkaria field and there are fewer intrusions at depth. The alteration intensity of the rocks in OW 927B tends to increase with depth in near surface layers and then decrease at depth with trachyte being only slightly altered while the interlayers of basalt, tuff and breccia are highly altered. The trachyte in the deeper parts of the well is massive and aphanitic with minor clay alteration. Hydrothermal alteration minerals in the well are divided into five zones: unaltered 0-162 m, zeolite-illite zone 162-492 m, chlorite-illite zone 492-916 m (220°C), epidote-chlorite-illite zone 916-1090 m (240°C) and actinolite-epidote-chlorite-illite zone 1090-2990 m (280°C). The alteration minerals fluorite and hematite suggest cooling in the deeper parts of the well.

Clay alteration minerals consist of kaolinite, mixed layer clay, illite, and chlorite. Clay minerals were analysed with SEM-EDS in microprobe and XRD in three different rock types, basalt, rhyolitic tuff and sedimentary tuff. Compositional variations were revealed: basalt contains chlorite and interlayered chlorite-illite clay, rhyolitic tuff contains interlayered illite-chlorite clay and sedimentary tuff contains Fe-rich chlorite.

## **1. INTRODUCTION**

In geothermal exploration and exploitation hydrothermal minerals are important tools for assessing the physical and chemical properties of a geothermal system, such as temperature, rock permeability and fluid acidity or fluid rock interaction (Browne, 1970; Elders, 1977; Reyes, 1990).

The objective of this study is to restructure the well stratigraphy of well OW 927B, to determine the distribution of alteration minerals within the well, and, furthermore, to investigate the chemical composition of clay minerals in the well in relation to different rock types. The information is used to evaluate the potential of the geothermal resource for further expansion within the area the well has explored. OW 927B is located south of the Domes field and is deviated to the south towards the southern edge of the field. Kenya Electricity Generating Company PLC purchased the land south of Olkaria Domes in line with the company's geothermal expansion strategy. The land is outside the geothermal license area and the company is currently in the process of acquiring geothermal licenses for the said parcel of land. Geo-scientific investigations are already underway in the newly acquired land.

## 2. GEOLOGY

### 2.1 Geological setting

The Kenya Rift, which extends from Turkana in the north to the central Tanzania plateau (Figure 1), displays several N-S and NNW-SSE trending faults (Smith and Mosley, 1993). Using chronologic and lithostratigraphic correlation methods, Thompson and Dodson (1963) and Baker and Wohlenberg (1971) were able to categorise the volcanic and structural development of the Kenya Rift. Volcanism in the Miocene period marked the onset of the opening of the rift. During the late Miocene faulting of the rift started, followed by the eruption of large volumes of Pliocene ignimbritic tuff, which coincidentally caused the development of a depression in the central segment of the rift (Omenda, 1998).

The Kenya Rift Zone is divided into three distinct graben sectors (Smith and Mosley, 1993). The north graben sector extends from Lake Turkana in the north to Lake Bogoria trending NNE-SSW. Second is the central graben sector, which extend from Menengai to Suswa, and is a well-defined 50-70 km trough with narrow faulted western margins and a faulted platform in the east. The inner trough is cut by a series of N-S trending left-stepping, en echelon fault zones (Baker, 1986). The third sector is the southern graben sector characterized by the absence of rift floor faulting. It stretches from south of Lake

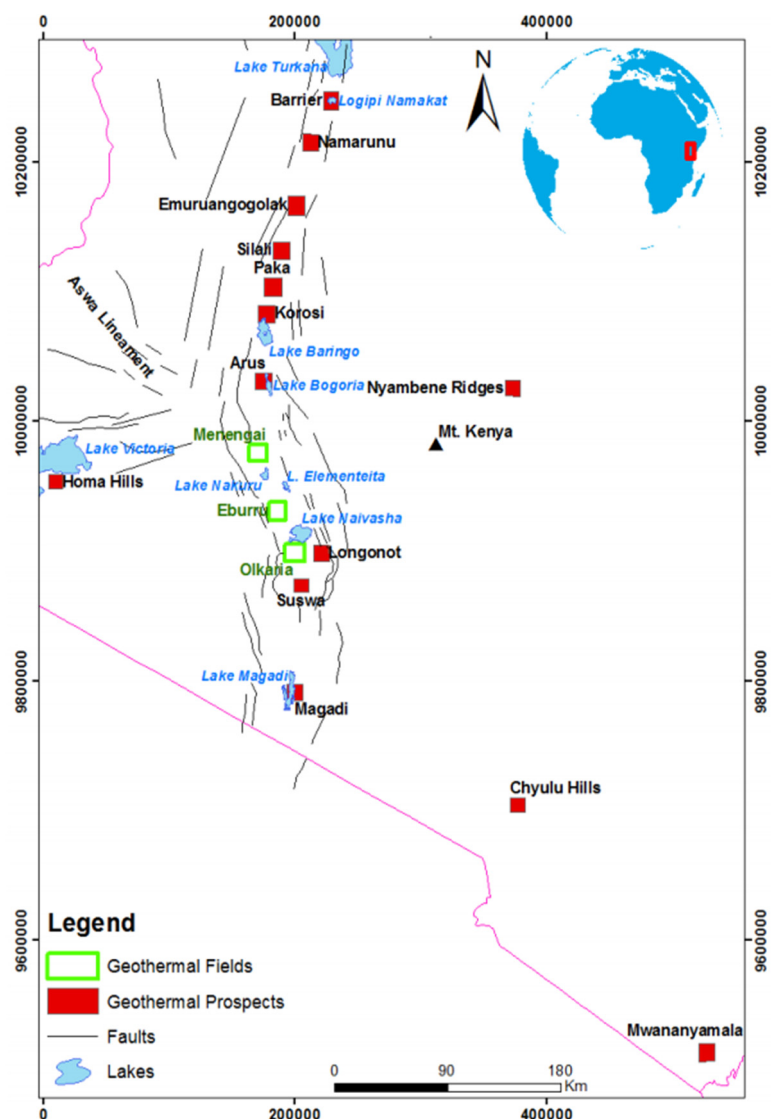


FIGURE 1: Simplified map of the Kenyan rift showing location of geothermal prospects and fields (Clarke et al., 1990, modified by Simiyu, 2010)

Magadi to Tanzania and is 200 km wide with a low relief zone of normal faulting. The Olkaria volcanic complex is located in the central graben sector; it comprises trachyte lavas, comendites (rhyolitic lavas) and domes covered with pyroclastic deposits. The calderas and the ring structures show an E-W to WNW–ESE trend (Clarke et al., 1990). The ring structure is formed by arcuate rhyolitic domes to the east and southwest of Olkaria Domes geothermal field (Figure 2).

## 2.2 Structural setting

The Olkaria complex lies within the trough in the central segment of the Kenyan Rift and covers an area of 240 km<sup>2</sup> where multicentred volcanic fields and at least 80 small volcanic centres have been identified (Clarke et al., 1990) (Figure 2). The structural fault systems within Olkaria geothermal field include NW-SE, N-S, E-W and ENE-WSW structures.

The NW-SE structures are believed to be the oldest structures and are affiliated with the development of the rift (Lagat, 2004). The fault extends from Gorge farm near the northeast field to Oloidien bay near the east production field and from there into the northeastern sector of the Olkaria Domes field (Figure 2). The ENE-WSW trending faults (Olkaria fault zone) and NW-SE faults (Gorge farm) are old, rejuvenated structures. The Olkaria fault is observable on the surface by the manifestation of fumaroles and alteration of ground, which includes silicification and sulphur encrustations (Omenda, 1998).

The youngest faults are N-S faults and fractures. NE-SW and NNE-SSW trending faults are associated with latter tectonic activities. Along the Ol-Njorowa gorge, N-S trending dykes and volcanic necks are exposed suggesting that faulting played a key role in the initiation of the gorge. Vertical permeability is attested by the occurrence of strong fumarolic activity along the gorge (Otieno et al., 2014). The most important structure in the Olkaria volcanic complex is the alignment of rhyolitic domes, which indicates the presence of a buried caldera (Naylor, 1972; Clarke et al., 1990; Mungania, 1992). The exposure of geological surface structures is limited in the Domes field due to a thick cover of pyroclastic deposits. Most structures are deduced from mapping of deep gullies and stratigraphic correlation of drilled wells (Lagat, 2004). Cavings and total loss of circulation during drilling have also served as a clear indicator of the existence of sub-surface faults structures (KenGen, 2012). Geothermal manifestations are strongly associated with structural features, for example the fumaroles concentrated along the ring structure on the eastern side of Olkaria Domes and along the N-S trending fault (Clarke et al., 1990; Mungania, 1992; Lagat, 2004).



FIGURE 2: Structural map of Greater Olkaria geothermal area with volcanic centre (KenGen, 2012; Okoo, 2013)

### 2.3 Lithology of Olkaria geothermal field

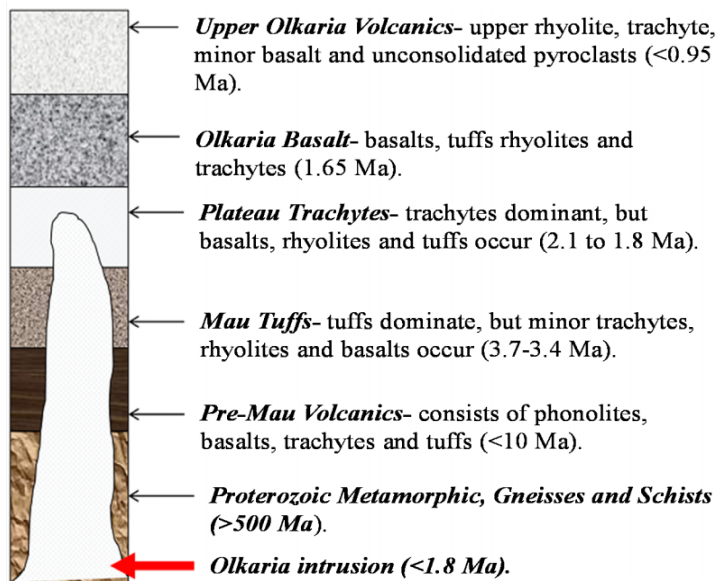


FIGURE 3: Modified sub-surface litho-types of the Olkaria geothermal field (Omenda, 1998)

The Olkaria volcanic complex is characterized by numerous volcanic centres of Quaternary age, which form steep-sided domes consisting of lavas and pyroclastics (Macdonald et al., 1987). Lagat (2004) noted that the Olkaria volcanic complex is the only area in the Kenya rift where comenditic lavas occur. Generally, the lithostratigraphy of the Olkaria geothermal field is as described in Figure 3. The basement system of gneisses and schists is the oldest formation, followed by the Mau tuffs formation, which is the oldest rock encountered in Olkaria and correlates with tuffs of Mau of Pliocene age (Omenda, 1998).

Plateau trachyte forms part of Kenya rift floor fissures, which are exposed to the south and north of the Olkaria

volcanic complex. The Pleistocene rocks of the Plateau trachyte formation occur in the east sector of the field. The formation is dominated by trachyte, but rhyolite, basalts and tuffs can be found. The absence of Plateau trachyte to the west of Olkaria hill indicates that late Pleistocene magmatic activity occurred in the N-S rift fault. The formation hosts the geothermal reservoir in the Olkaria geothermal field. The permeability is a consequence of abundant late Pleistocene N-S grid faults and rejuvenation of the older ENE faults (Omenda, 1998).

Olkaria basalt is younger than 1.65 Ma; the formation consists of several thin basalts separated by thin layers of tuff, minor trachyte and rare rhyolites. The formation is moderately to highly altered with clays, calcite and epidote being the alteration products (Omenda, 1998). Low permeability of units is associated with minimal faulting and deposition of secondary minerals as the formation marks the interface between cool groundwater and upwelling hot fluids. It is believed to form the cap rock for the Olkaria geothermal system (Haukwa, 1984; Ambusso and Ouma, 1991; Otieno and Kubai, 2013).

Upper Olkaria volcanics are the youngest units and are dated to less than 0.95 Ma (Omenda, 2000; Lagat, 2004). The rocks comprise comendites, trachyte and minor basalt (Thompson and Dodson, 1963; Clarke et al., 1990; Omenda, 1998). The youngest lavas of the Olkaria volcanics are the Ololbutot comendites, which are dated to 180 +/- 50 years and erupted from a N-S oriented fissure. The eruption of lavas and pyroclastics are structurally controlled mostly by eruptive centres along N-S fissures and the ring structures (Clarke et al., 1990). The stratigraphy of the Domes field corresponds to the stratigraphy of Greater Olkaria volcanic complex. Studies done by Lagat (2004), Musonye (2012) and Ronoh (2012) showed that Olkaria Domes comprise Upper Olkaria volcanics, followed by Olkaria basalts and proceeded by Plateau trachytes with intrusions.

### 3. SAMPLING AND ANALYTICAL METHODS

In the absence of conventional core data, drill cuttings provide a continuous, independent and cheap data source. Data collected from drill cuttings can be used to update conceptual models of geothermal

systems by determining the permeability, porosity, and lithology type, by locating fractures or faults and by assisting with petrophysical characterization. For well OW 927B, which is located in Olkaria Domes, drill cuttings were collected every 2 m while noting the time, the inflow and outflow temperatures, and the deviation angle.

### **3.1 Binocular analysis**

At the rig site, preliminary analysis was carried out by the rig geologist using the binocular microscope mainly to identify the rock type and alteration mineralogy. The result was used to decide the depth of the production casing. More detailed analysis with an Olympus binocular microscope was done at the laboratory of ÍSOR – Iceland GeoSurvey in order to reconstruct the stratigraphy of OW 927B. Properties such as the primary rock forming minerals, colour of the rock, texture and grain size of the rocks, presence of alteration minerals, zonation or paragenesis of mineral sequences and intensity of alteration were determined.

### **3.2 Petrographic microscope analysis**

In total, 12 thin sections of OW 927B cuttings were prepared at the University of Iceland and were analysed using the LEICA DM 2700P petrographic microscope at ÍSOR's laboratory. The petrographic microscope used for analysis is fitted with 5 objective lenses of different magnifications (x5, x10, x20, x40, and x63). The thin sections are of normal standard of 30  $\mu\text{m}$  thickness, but without cover glass. The x5 objective lens was used to survey the whole thin section and locate areas of interest. The areas of interest were then magnified with x10 and x20 lenses to observe more closely and to take images. The optical images shown in the study were photographed using an Olympus UC 30 camera coupled with Stream start software. The purpose of the petrographic analysis was to confirm the rock type, intensity of alteration and the alteration minerals and to study the evolution of the alteration mineral sequences within fractures, vesicles and veinlets in the thin sections. The petrographic analysis also enabled mapping of clay minerals in the thin section, which were later analysed using the electron microprobe.

### **3.3 X-Ray diffraction (XRD) analysis**

Clay minerals belong to the phyllosilicate group and their formation occurs both under surface and subsurface conditions. The phyllosilicates are usually fine-grained minerals, making it difficult to identify them without using either a petrographic microscope, XRD or electron microprobe. However, they have been studied in great detail by X-ray diffraction, which is the basic tool for their identification (Meunier, 2005). The X-ray diffractometry analysis is based on the principles of Bragg's law where a beam of X-rays is passed through a particular mineral and geometric conditions are achieved. The X-rays scattered from the crystalline sample interfere, producing a diffraction peak. In this study, a total of 10 samples were selected based on different lithologies, then prepared at ÍSOR's laboratory (Appendix I) and analysed at the University of Akureyri in northern Iceland.

### **3.4 Electron microprobe analysis**

Electron microprobe analysis (EMPA) is an analytical technique, which can be traced back to the discovery of X-rays (Castaing, 1951). The X-rays can be detected with either an energy dispersive spectrometer (EDS) or a wavelength dispersive spectrometer (WDS). EMPA is used to determine the elemental composition of solid specimens and is also able to produce backscattered images, maps and measure their concentration. After the petrographic analysis, four thin sections were selected for chemical analysis of clay minerals. The thin sections were carbon coated to create a conducting surface for imaging and analysis of the sample. They were analysed using a JEOL JXA-8230 super probe with

acceleration voltage of 15 kV and a beam current of 10 nA at the Institute of Earth Sciences at the University of Iceland. Due to limited time, only three of four thin sections were analysed using EDS, whereby chemical components in oxides weight percentages were determined and backscattered images and maps were created.

#### 4. BOREHOLE GEOLOGY

##### 4.1 Drilling of well OW-927B

Well OW 927B is located at 9898589.514 northing and 202413.224 easting at an elevation of 1981 m, which is within the Olkaria Domes production field (Figure 4). The well was spudded on 23<sup>rd</sup> January 2016 and completed on 17<sup>th</sup> March 2016 after a period of 52 days, reaching a total depth of 2990 m while being deviated to the north (Table 1). The aim of drilling the well was to confirm the extent of the resource in the southern part of the Domes field and to provide steam for Olkaria IV power plant.

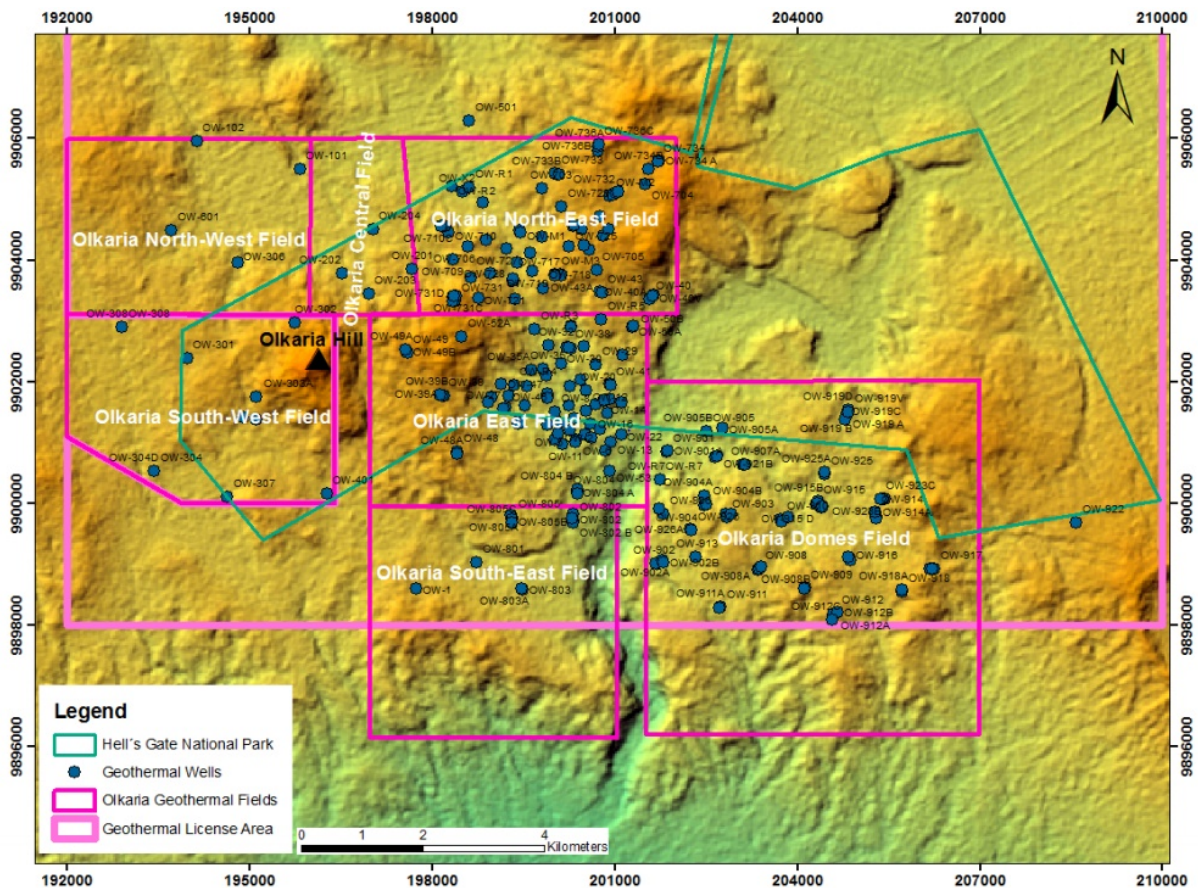


FIGURE 4: Map of the Olkaria geothermal area showing the location of well OW 927B in Olkaria Domes field (Otieno and Kubai, 2013; modified by Otieno, 2016)

TABLE 1: Drilling phases and casing design for well OW-927B

Stage	Hole diameter (")	Depth (m CT)		Casing	
		From	To	Casing diameter (")	Type
Phase 1	26	0	56	20	Surface
Phase 2	17 <sup>1</sup> / <sub>2</sub>	56	292	13 <sup>3</sup> / <sub>8</sub>	Anchor
Phase 3	12 <sup>1</sup> / <sub>4</sub>	292	992	9 <sup>5</sup> / <sub>8</sub>	Production
Phase 4	8 <sup>1</sup> / <sub>2</sub>	992	2990	7	Slotted liners

### 4.1.1 Phase 1: Drilling of surface hole

A surface hole was drilled with a 26" roller cone milled tooth bit using bentonite-based mud to a depth of 56 m CT (cellar top). Full circulation returns occurred at the surface throughout the drilling of this phase. It was cased using a 20" diameter surface casing.

### 4.1.2 Phase 2: Drilling of the intermediate hole

Drilling stage 2 involved using a 17<sup>1</sup>/<sub>2</sub>" roller cone bit with aerated water and foam as the drilling fluid. Minor loss of returns over 152-162 m depth and a low rate of penetration (Figure 5) were experienced during this phase. The hole was circulated before the 13<sup>3</sup>/<sub>8</sub>" anchor casing was run in hole and the casing shoe set at 292 m CT.

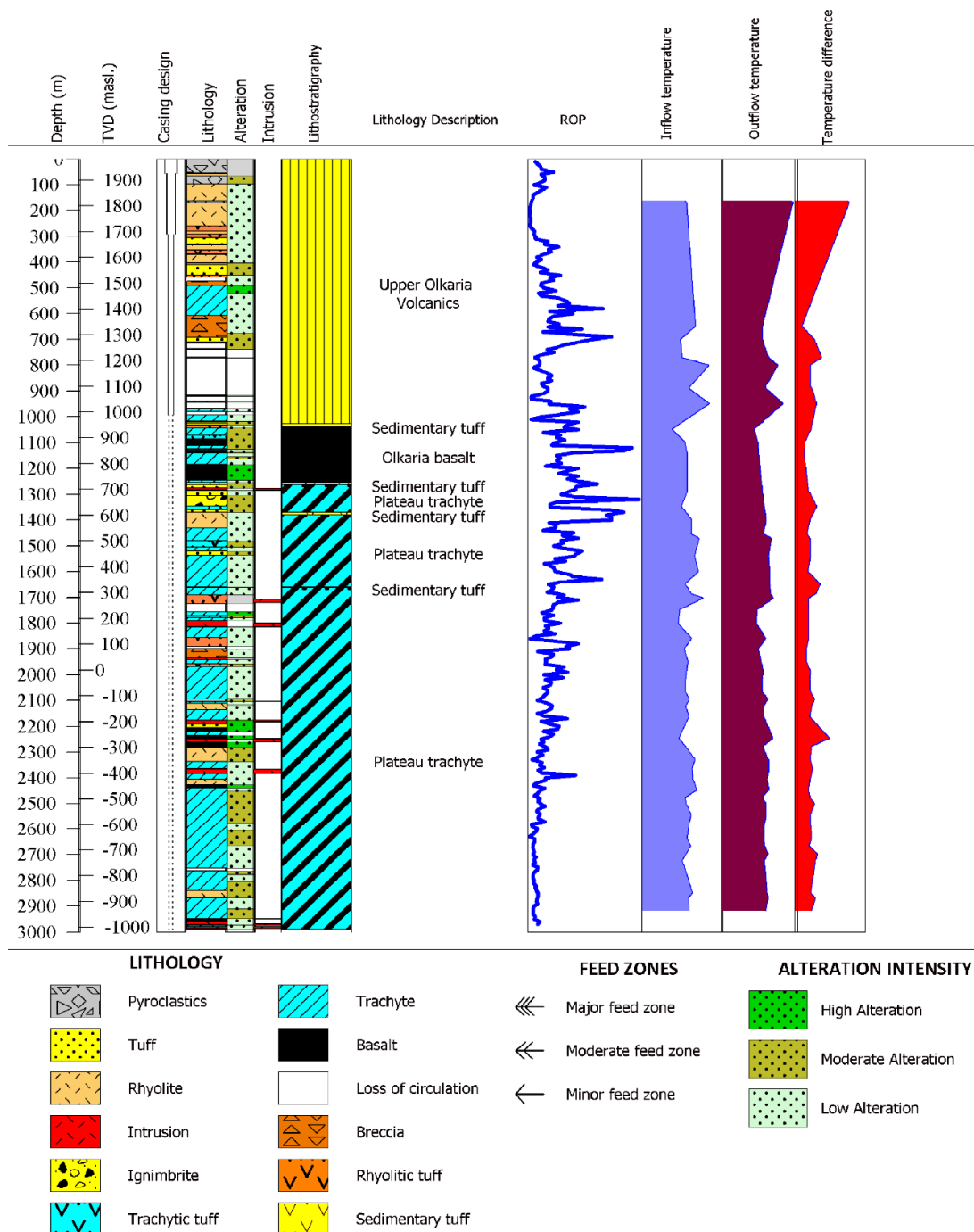


FIGURE 5: Lithology, lithostratigraphy, rate of penetration (ROP), inflow, and outflow temperatures

### 4.1.3 Phase 3: Drilling for production casing

This phase using a 12<sup>1</sup>/<sub>4</sub>" roller cone bit began smoothly, with full circulation of returns received at surface. Major loss of circulation returns was experienced from 660 m CT to the casing shoe at 992 m CT. Run in hole (RIH) of the 9<sup>5</sup>/<sub>8</sub>" outer diameter (OD) production casings was followed by cementing and three backfills.

### 4.1.4 Phase 4: Drilling of production section

Drilling at this phase resumed with a 8<sup>1</sup>/<sub>2</sub>" roller cone bit, with aerated water and foam as the drilling fluid. The drilling of the well progressed with minor loss of circulation. The final depth of 2990 m CT was achieved on 15<sup>th</sup> March 2016. The crew embarked on circulating the wellbore with water before RIH of the 7" perforated liner.

## 4.2 Lithology of OW 927B

The lithology of well OW 927B has been categorised into three lithostratigraphic formations in accordance with previous studies (Omenda, 1998) (Figure 3), which are the upper Olkaria volcanics (pyroclastics, rhyolite, tuff, breccia), the Olkaria basalts (basalts with intercalation of thin layers of tuff and trachyte) and the Plateau trachyte (trachyte with intercalation of tuff, basalt and some minor intrusions) (Figure 5). The classification of the rocks is based on the presence of the primary minerals quartz, plagioclase and sanidine feldspar, olivine, pyroxene and the general crystallinity, as well as heterogeneity and/or homogeneity of the rock sample.

### 4.2.1 Upper Olkaria volcanics (0-1026 m CT)

Upper Olkaria volcanics is the formation between the surface and 1026 m CT depth (Figure 3), but thickness can be variable from 0-1200 m between wells in the Domes area or the Olkaria geothermal field. It comprises comendites (rhyolites) and pyroclastics and belongs to the most recent volcanic activity. It is believed that the pyroclastics originate from the Longonot volcanic centre while the comendites originate from the volcanic centres of Olkaria Hill, the Ololbutot volcanic fissure and the Gorge farm (Clarke et al., 1990). Horizons of sedimentary tuff in the well are used as marker horizons between the episodic volcanic periods during the evolution of the Olkaria volcanic complex.

*0-96 m – Pyroclastics:* Forms the uppermost part of the well; they are brown to yellowish in colour with a mixture of unconsolidated fragments comprising volcanic glass, pumice, rhyolite and tuffaceous material. The formation is moderately oxidized with no alteration minerals occurring. A thin layer of rhyolite is noted between 56-66 m, which is highly porphyritic with quartz phenocrysts.

*96-494 m – Rhyolite:* Whitish to green highly porphyritic rhyolite with an abundance of quartz phenocrysts. Fragments of pumice are noted at certain intervals. The rock is vesicular and mild oxidation is noted. Under the petrographic microscope the rock appears crystalline with flow textures. It is slightly fractured with zeolite, clays, pyrite, chalcedony, and quartz precipitating in the fractures at 492-494 m. Most of the glass below 334 m has started to alter into clays with slight alteration intensity. Both pyrite cubes and dissemination are abundant. Intercalations of tuffaceous rock are observed at 48 m and of rhyolitic tuff at 192 m.

*494-606 m – Trachyte:* Light green, fine grained porphyritic rock. Calcite noted. The formation is highly altered to green clays. Pyrite disseminations noted in the matrix. Micro-veining with pyrite and oxide infilling, high oxidation noted at 528-536 m indicating an aquifer or possibly cold inflow in the well. Partial losses at 540-546 m and 570-578 m.

*606-736 m – Breccia:* The sample cuttings analysed in this zone consist of heterogenous, angular fragments of tuffs, trachyte, rhyolite and basalt, which have been cemented together in a fine-grained glassy matrix. Under the binocular microscope it is observed that the brecciated fragments are highly altered to green clays. Loss of circulation was noted at 714-736 m.

*736-916 m – Rhyolitic tuff:* Light green to white, homogenous and crystalline rock. In petrographic analysis, fluorite is observed as a phenocryst. Most glass is altering to clays while oxides are altering to sphene and pyrite. Moderate alteration is noted. A sequence of mineralogy is observed where quartz infills a fracture and later fluorite is deposited. Major loss of circulation at 738-770 m and at 776-916 m.

*916-920 m – Basalt:* Grey to green, heterogenous fine-grained rock. The rock is highly altered to green clays. Fragments of basalt and tuff. Calcite is abundant. Epidote crystals appear first at 918 m depth. Loss of circulation at 920-940 m.

*940-1026 m – Trachyte:* White to brownish grey, fine grained, slightly altering to green clays. Slightly oxidized. Feldspars observed altering to epidote. Both pyrite cubes and dissemination noted to be embedded in the rock structure. Loss of circulation noted at 944-968 m.

#### **4.2.2 Olkaria basalts (1026-1254 m CT)**

Between the Olkaria volcanics and the Olkaria basalts, a thin layer of 12 m sedimentary tuff is observed. This is defined as a marker horizon between two episodes of volcanic eruptions: the upper Olkaria volcanics and Olkaria basalt sequence.

The Olkaria basalts consist of several thin layers of basaltic lava flows, separated by thin layers of tuff, trachyte and rare rhyolites. The basaltic rock is characterized by a weak vesicular, medium to fine matrix, which contains porphyritic with augite and plagioclase. Mafic minerals are altered, and calcite and epidote are dominant at this zone (Omenda, 1998). The sample cuttings from 1030-1034 m, 1076-1086 m and 1158-1164 m are observed to be highly oxidized and the intensity of alteration is high to medium with numerous veining compared with other zones.

*1026-1038 m – Sedimentary tuff:* Brown to grey, heterogenous fragments of medium to fine grained tuff. It is highly oxidized and moderately altered. Coarse grained clays are observed. Cementation of white fragments are noted. The alteration minerals of epidote and chlorite are noted at this depth.

*1038-1044 m – Rhyolitic tuff:* Greenish, fine grained, very glassy, and highly vesicular tuff with phenocrysts of quartz. Alteration minerals include quartz, clays and epidote crystals as infilling in the vesicles. Both open and closed fracture veinlets were noted.

*1044-1086 m – Trachyte:* Grey to brown fine grained, slightly porphyritic with sanidine phenocryst. Most feldspars have been altered to green and brown clays. Numerous open fractures infilled with clays are noted with high oxidization. The rock is divided into massive and vesicular intervals. Epidote is the high temperature mineral noted at this depth.

*1086-1254 m – Basalt:* Dark green, medium grained, highly porphyritic basalt with plagioclase phenocrysts. The plagioclase phenocrysts are altering to clays. Alteration intensity is high. Platy calcite is noted. Highly fractured basalt with veins and vesicles infilled with epidote. A mineral sequence of clay-epidote-actinolite indicates prograde alteration in this zone. Petrographic analysis shows that olivine has been replaced by chlorite, plagioclase is altering to chlorite, calcite and albite, pyroxene is altering to actinolite, and oxides are replaced by sphene. Other alteration minerals observed include numerous fluorites and prehnites. At 1144-1186 m depth a 42 m thick layer of highly oxidized and highly porphyritic trachyte with sanidine phenocryst is observed.

### 4.2.3 Plateau trachyte (1254-2990 m CT)

The formation is dominated by trachyte with intercalation of rhyolite, basalts, and tuff. The trachyte can be subdivided into two types: One is strongly feldspar-phyric and dense and the other is fine grained, aphyric with trachytic texture (Omenda, 1998). In this study the trachyte is divided into two formations based on a thin sedimentary tuff layer, which represent the horizon marker between two different volcanic episodes, medium to highly porphyritic trachyte and poorly aphyric textured trachyte.

*1254-1264 m – Sedimentary tuff:* Reddish brown to grey, heterogenous fragments of tuff and trachyte. It is highly oxidized and altered to brown clays.

*1264-1306 m – Tuff:* The formation is grey to brown, fine grained and it is altered to green and brown clays. Coarse grained clays are noted infilling fractures veins, the formation is moderately oxidized and highly vesicular felsite rock is observed at 1274-1284 m.

*1306-1346 – Ignimbrites:* Brownish, fine grained, rock with fiamme texture. Denser ignimbrite is slightly fractured with veinlets that are filled with quartz infill. The ignimbrite is moderately altered and highly oxidized.

*1346-1370 – Tuff:* Greenish, fine-grained tuff is moderately altered to green clays. Feldspar is noted to be altering to adularia and chlorite. The alteration minerals assemblages include fluorite, quartz, sphene, adularia and chlorite. Fragments of pumice noted.

*1370-1380 – Sedimentary tuff:* Greenish, porphyritic with quartz and feldspar phenocryst. Fluorite is abundant and is found to be growing in fractures and veins. Pumice and fragments of ignimbrite are present. Part of the plagioclase is altering to clay and sanidine is noted to be altering to adularia and chlorite. Olivine is altering to oxides at the edges. The alteration minerals present are fluorite, quartz, sphene, adularia and chlorite.

*1380-1660 – Trachyte:* Grey to brown fine grained, porphyritic trachyte with sanidine phenocrysts. It is slightly altered to brown clays. Mild oxidation is noted. Fracturing noted at 1380-1432 m depth with quartz infills together with fine- and coarse-grained clay. At 1490-1504 m there is 14 m of trachytic tuff which is highly oxidized and highly vesicular.

*1660-1662 – Sedimentary tuff:* Reddish brown to grey cryptocrystalline rock, the rock is moderately altered and highly oxidized. It is dense and very massive. Numerous veins are noted.

*1662-1792 – Trachyte:* Brown to grey fine grained moderately porphyritic trachyte with sanidine phenocryst. The rock is slightly altered and moderately oxidized. Highly vesicular with coarse grained clay infilling the vesicle. At 1690-1720 m, a relative massive and fresh felsite rock is noted. Alteration minerals are actinolite, wollastonite, and epidote.

*1792-1814 – Microgranite:* Grey, fine grained. Slightly porphyritic with quartz phenocrysts. Presence of dark spikes noted. The rock is massive and fresh.

*1814-1856 – Trachyte:* Brown, fine grained, moderately porphyritic with sanidine phenocrysts. The rock is slightly altered. Alteration minerals noted are actinolite and prehnite.

*1856-1934 – Tuff:* A 34 m thick layer of tuff which is homogenous and brown in colour. Fracturing is noted. A mineral sequence is observed where chalcedony is replaced completely by quartz. Lithic tuff with heterogenous fragments of tuff and trachyte. Alteration mineralogy includes actinolite and epidote.

*1934-1950 – Syenitic intrusion:* Brown medium grained, syenite which is composed of alkali feldspars. The rock is relatively fresh.

1950-2216 – *Trachyte*: Grey, fine grained moderately porphyritic trachyte with sanidine phenocryst. The rock is massive and relatively fresh with minor clays noted. Wollastonite and epidote occur as high temperature minerals. At 1958-1968 m, a 10 m unit of rhyolitic tuff which is green to white and fine grained is noted. Intercalation of rhyolitic intrusion, basalt, rhyolite, and tuff is noted at this depth.

2216-2240 – *Basaltic dyke*: Dark green fine-grained basalt. The rock is highly altered to green clays. It is fractured with veinlets infilled with epidote. Pyroxene is replaced by amphiboles like uralite. The formation is highly oxidized. With intercalation of trachyte and highly altered basaltic rock. Alteration minerals are clay, actinolite, prehnite and epidote.

2240-2262 – *Syenitic intrusion*: Grey, fine grained to medium grained syenitic dyke. The rock is slightly altered to green clays. The formation is slightly altered with actinolite and epidote replacing some of the primary minerals.

2262-2284 – *Basalt*: Dark grey, fine to medium grained basalt. The rock is massive and moderately altered to green clays. Fractured with epidote quartz vein filling.

2284-2340 – *Felsite/rhyolitic intrusion*: Whitish to green fine grained highly felsic rock. Some of the fragments are slightly altered and others are relatively fresh. Fractures are filled with green clays. Epidote and actinolite are common alteration minerals. Vesicle showing mineral zoning of quartz and chlorite in binocular analysis of 2302-2304 m.

2340-2364 – *Trachyte*: Light grey to light green, fine-grained trachyte. Slightly porphyritic with sanidine phenocrysts. It is slightly altered to green clays.

2364-2382 – *Syenitic intrusion*: Pinkish to whitish, fine grained to medium grained syenite rock. Most of the pyroxene are altered to clays and epidote. The rock is fractured with infilling veins. Alteration minerals are actinolite and epidote.

2382-2406 – *Trachyte*: Grey, fine grained, slightly porphyritic trachyte with sanidine phenocrysts. The rock is slightly altered. Minor amounts of epidote observed.

2406-2426 – *Rhyolite*: Whitish, fine grained felsic rock. It is slightly altered to green clay. Numerous veins are noted. Epidote commonly replace feldspars.

2426-2440 – *Basalt*: Dark green fine grained to medium grained basalt. The rock is highly altered to green clays and veining is scarce.

2440-2840 – *Trachyte*: Light-grey, fine to medium grained trachyte. The rock is weakly to moderately porphyritic with sanidine phenocrysts. The formation is moderately vesicular with infills of green clays and actinolite. Actinolite is abundant and is observed replacing pyroxenes. The rock is moderately altered. Veining is also observed with infills of actinolite and clays. Light grey, whitish, fine grained felsic rock at 2532-2546 m. It is slightly altered to green. Veining is noted.

2840-2910 – *Rhyolite*: Light grey to pale green, highly porphyritic rhyolite with large quartz phenocrysts. Feldspar phenocrysts are also observed. It is fine to medium grained and moderately altered to pale green clays. Micro veins infilled with green minerals are noted.

2910-2968 – *Trachyte*: Grey to dark grey, fine grained, weakly porphyritic rock with sanidine phenocrysts. Micro veins are observed. Minor oxidation observed in some fragments. Interlayer of 10 m thick unit of basalt with platy calcite is observed at 2952-2954 m.

2948-2950 – *Rhyolitic intrusion*: Light grey to whitish fine grained weakly porphyritic with minor quartz phenocrysts. The formation appears massive and fresh. Slight alteration is noted.

2968-2974 – *Basalt*: Dark grey, medium grained basalt with abundant epidote. The formation is highly altered to green clays.

2974-2980 – *Trachyte*: Brown to dark grey, fine grained, slightly porphyritic trachytic lava with micro veins in-filled with quartz. Formation is slightly altered to green clays.

2980-2986 – *Syenite intrusion*: Light grey to whitish fine grained weakly porphyritic rock with minor quartz phenocrysts. The formation appears massive and fresh. Slight alteration noted.

2986-2990 – *Trachyte*: Brown to dark grey, fine grained, slightly porphyritic trachytic lava with micro veins in-filled with quartz. Formation is slightly altered to green clays.

## 5. HYDROTHERMAL ALTERATION MINERALOGY

Hydrothermal alteration is the mineralogical change that results from fluid-rock interaction, which is controlled by variations of the fluid composition, temperature and pressure. For hydrothermal alteration to occur in a certain area, the presence of a heat source and rock fractures are essential. The heated water has a lower density and is able to rise along fractures. The circulating fluid can involve meteoric or sea water. Hydrothermal fluids, formed by hot fluid-rock interaction (Browne, 1970) are related to temperature and permeability. In Olkaria, the first appearance of epidote is used to determine the reservoir depth (Bird and Spieler, 2004). The typical hydrothermal alteration minerals replacing primary minerals are listed in Table 2.

TABLE 2: Typical hydrothermal alteration replacement products. Modified from Browne (1982).

Original mineral or phase	Replacement Products
Volcanic glass	Zeolites, cristobalite, quartz, calcite and clays
Magnetite	Pyrite, sphene, pyrrhotite, hematite
Pyroxene, amphibole, olivine, biotite	Chlorite, illite, quartz, pyrite, calcite, anhydrite
Calcic plagioclase	Calcite, albite, adularia, wairakite, quartz, chlorite, illite, epidote
Anorthoclase, sanidine, orthoclase	Adularia

### 5.1 Rock forming minerals in the well and their alteration

*Volcanic glass* is formed when magma extruded onto the surface is cooling rapidly having no time to form crystals. It is therefore highly susceptible to alteration, is very unstable and tends to change easily from magma to a crystalline state. Volcanic glass is the first to get altered and replaced by clays, zeolites, calcite and other minerals (Table 2). In thin sections from well OW 927B, volcanic glass is characterized by perlitic texture and is observed in rhyolites and in rhyolitic fragments in tuff and breccia at 334-336 m and 492-494 m.

*Olivine* occurs as a primary mineral in basaltic rocks and alters to form clays, quartz and calcite. In petrographic analysis, it often appears euhedral and is colourless or yellowish in plain polarized light but appears with 2<sup>nd</sup> order interference colour in crossed polarized light. The mineral is anisotropic with a parallel extinction angle. Olivine pseudomorphs were observed at 916 m, 1096 m and 2192 m in basalt and tuff formations but were completely replaced by chlorites.

*Feldspars* are the most dominant rock forming primary minerals both in trachyte and basalt. In OW 927B, feldspars occur as alkali feldspars, mainly as sanidine, which is common in trachyte (Figure 6).

The other group is the plagioclase feldspars, which are dominant in basaltic rock. The feldspars were milky whitish to colourless in color under the binocular microscope. In thin sections, it was colourless under plain polarized light (Figure 6d) and 1<sup>st</sup> order grey under crossed polarized light with simple and Carlsbad twinning (Figure 6c). At 736 m, sanidine phenocrysts are altered to adularia, and the plagioclase at 1096 m, a basaltic rock, is completely replaced by calcite, chlorite and actinolite. Other alteration mineral replacing the feldspar are adularia, sphene, prehnite and epidote.

*Quartz* is a primary rock forming mineral in rhyolitic rocks and granitic intrusions. It occurs both as phenocryst and in the groundmass and is resistant to alteration. In the study well phenocrysts of quartz were, e.g. observed at 334 m depth. In Figure 6 a and b, quartz phenocrysts are seen in the thin section. The quartz minerals are colourless with distinct fluid and melt inclusions. Under crossed polarized light, it exhibits undulating extinction from black and white to grey. Other distinguishing optical properties of quartz observed are that it is uniaxial positive and has low relief.

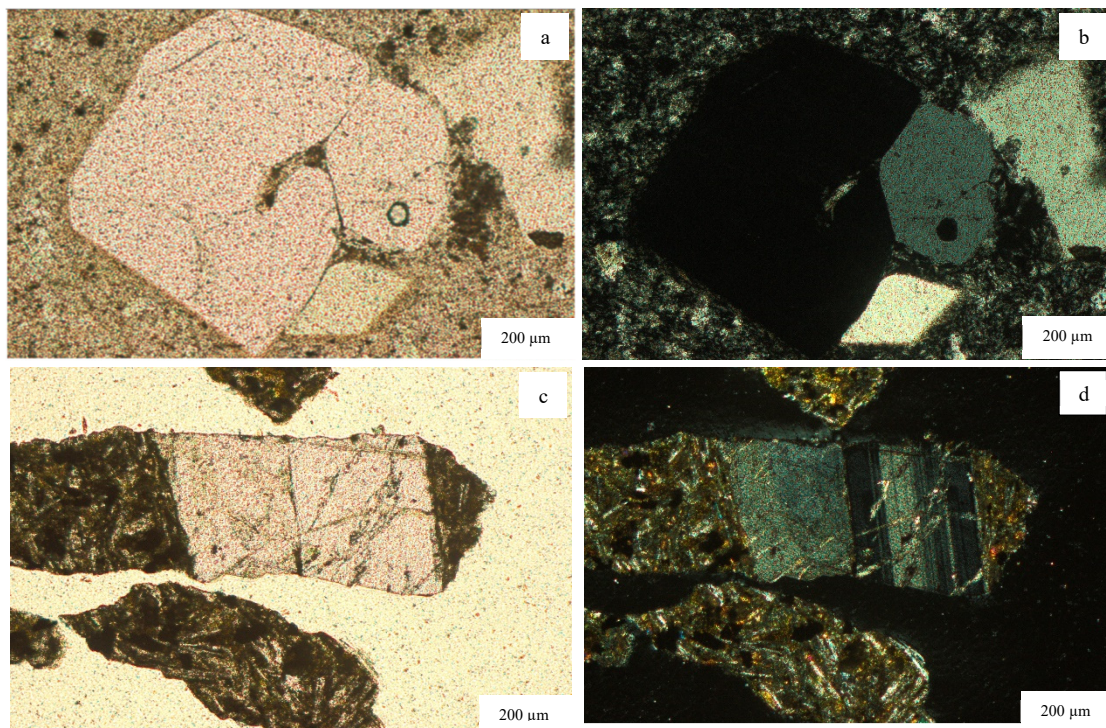


FIGURE 6: a) to d) Photomicrographs of quartz phenocryst and plagioclase feldspars as primary rock forming minerals. a) and c) under plain polarized light; b) and d) under crossed polarized light.

*Pyroxene*: Most of the pyroxene noted in this well are clinopyroxenes which include aegirine-augite and augites. In petrographic analysis, it is colourless in plane polarized light and yellowish, blue and orange in crossed polarized light. Zoning is noted in some of the pyroxene. It has a high relief and a maximum extinction angle of 90°. It forms as primary mineral but due to high temperature or hydrothermal fluids, it is gradually replaced by chlorite, actinolite, illite, quartz and sometimes calcite. At 916 m depth, pyroxene is partially altered at the edges of the mineral (Figure 7). Pyroxenes are completely altered to chlorite and actinolite at 1096 m depth.

*Fe-oxides*: Iron oxide colours the rock reddish due to its iron (Fe) content. It is commonly formed during the alteration of high ferrous mineral like olivine and pyroxene in basaltic rock. Iron oxide zones were found almost continuously from the surface down to 2450 m. Fe-oxides are observed to be fresh at 916 m and 1226 m depth, but at 1370 m and 1960 m depth Fe-oxides are observed to be altered to sphene, pyrite, epidote and actinolite.

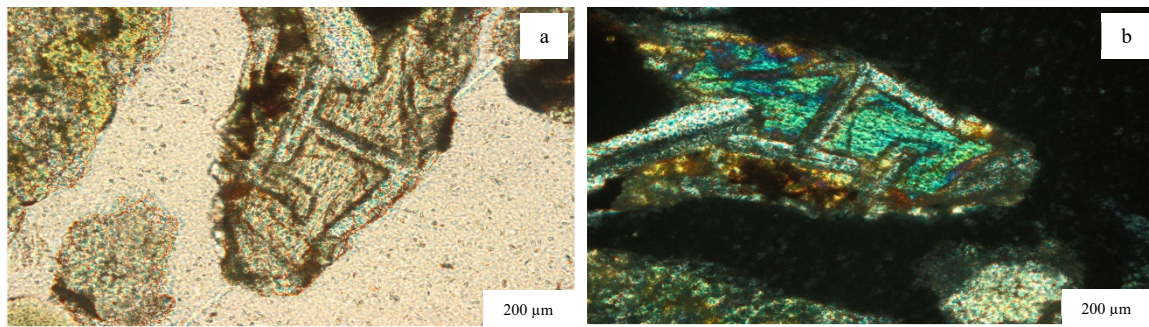


FIGURE 7: Photomicrographs of augite in basalt at 916 m a) under plain polarized light b) under crossed polarized light

### 5.2 Hydrothermal alteration mineralogy occurring in OW 927B

Hydrothermal alteration minerals in OW 927B occur as either precipitation or as a replacement of primary minerals (Figure 8). Secondary minerals precipitate in fractures, vesicles or vugs, when hot

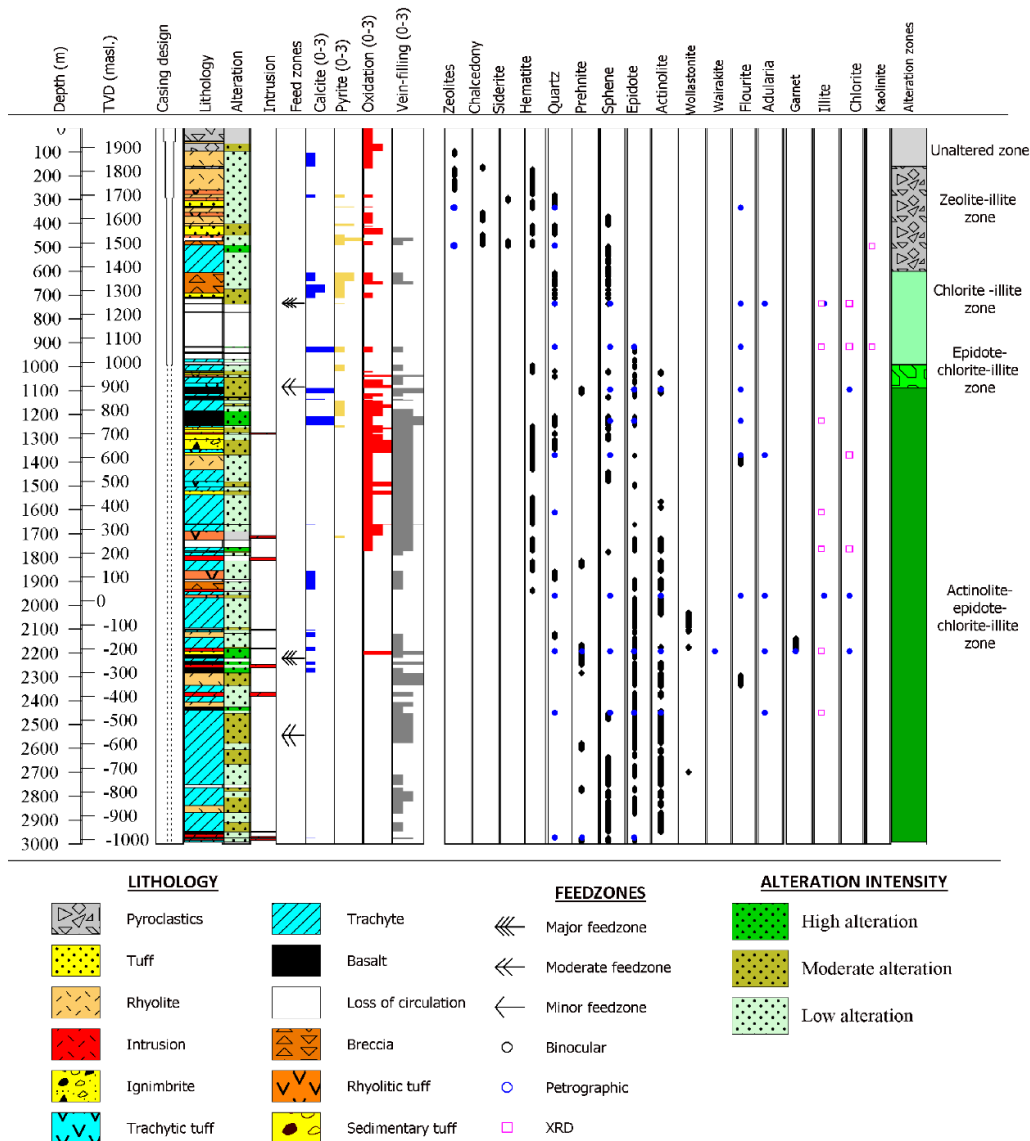


FIGURE 8: Distribution of permeability and alteration minerals observed in OW 927B

hydrothermal fluids circulate through the rock. Furthermore, replacement occurs when primary minerals are altered due to change in temperature and pressure conditions. The main alteration minerals observed in OW 927B are zeolites, chalcedony, hematite, fluorite, quartz, adularia, sphene, calcite, epidote, actinolite, wollastonite, wairakite, and garnet (Table 3). Clay minerals are discussed separately in section 6.

TABLE 3: Common hydrothermal alteration minerals used as geothermometers and their temperature stability ranges. Modified from Lagat (2004).

Mineral	Minimum temp (°C)	Maximum temp (°C)
Chalcedony	50	180
Calcite	20	<330
Pyrite	-	-
Chlorite	200	>350
Illite	200	340
Albite	180	320
Adularia	180	300
Quartz	180	350
Sphene	200	>350
Wairakite	220	>350
Prehnite	240	320
Epidote	240	>350
Biotite	270	>350
Actinolite	280	>350
Garnet	300	>350

*Zeolites:* The zeolites observed were noted to be replacing volcanic glass as well as occurring in fractures and vesicles as deposition. In petrographic analysis, the scolecite type of zeolite was identified, which appeared as grey acicular radiating crystals with spherical cluster of prismatic crystals (Figure 9). Zeolites were noted to occur at 334-336 m and 492-494 m depth. The zeolites identified in this well formed at temperatures below 100°C.

*Chalcedony* occurs from the surface to 920 m depth infilling vesicles in well OW 927B. It appears colourless, white in colour or sometimes bluish-grey and cryptocrystalline. Chalcedony is found lining vesicles as well as coating fractures and veins at 354-494 m depth (Figure 10). At 1856-1890 m depth, chalcedony is completely replaced by quartz, but the chalcedony outline is still preserved. Chalcedony forms at temperatures below 180°C.

*Calcite* occurs as a replacement of volcanic glass, plagioclase, and pyroxene, often as a precipitate in fractures and vesicles together with clay. Calcite occurs in abundance in the basaltic formations in the well but rarely in rhyolites and trachyte. Calcite is associated with boiling, dilution, and condensation. Simmons and Christenson (1994) found out that calcite can form during heating of cooler peripheral fluids. Calcite was observed to be abundant at 916 m depth in basaltic rock, which indicates possible boiling conditions,

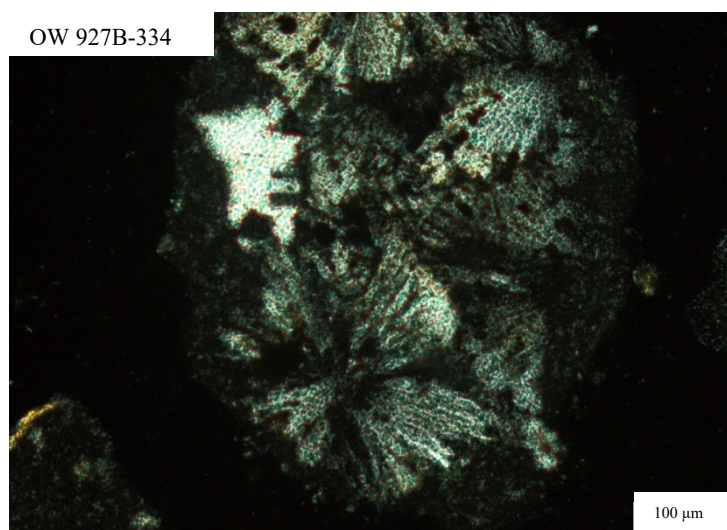


FIGURE 9: Photomicrograph of zeolite with grey acicular crystals under crossed polarized polars, possibly

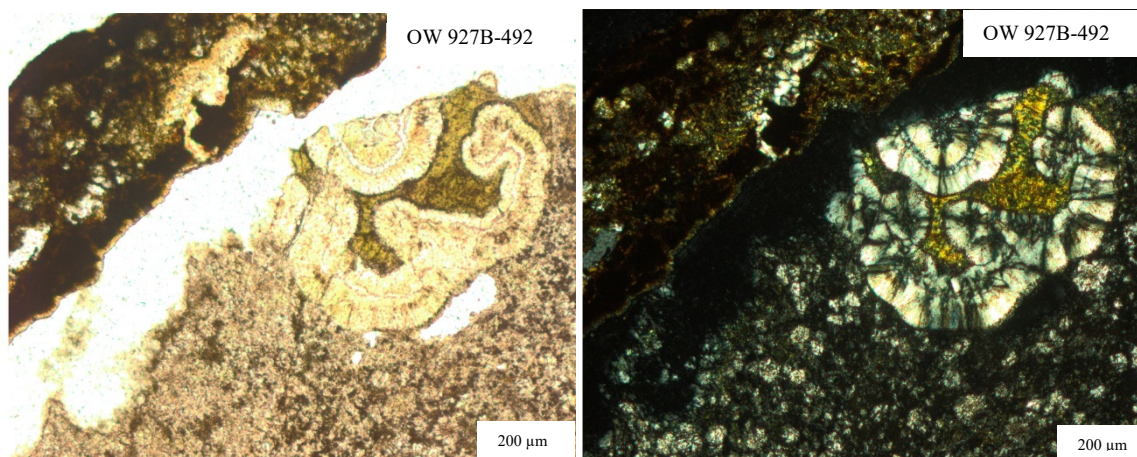


FIGURE 10: Photomicrographs showing chalcedony and green clays at 492 m: a) Plain polarized light; b) Under crossed polarized light

porosity, and permeability. In binocular analysis calcite appears white and when tested with 1 M hydrochloric acid it produces an instant, obvious fizz. In petrographic analysis, it appears transparent under plain polarized light but with high birefringence colour (4<sup>th</sup> order) in crossed polarized light. Other optical properties include rhombohedral, uniaxial negative, polysynthetic twinning and when rotating the mineral by 45 degrees, the mineral grain goes to a maximum extinction. In the sample cuttings, calcite occurs sporadically from 162 m to 1250 m and then disappears, occurring again from 1900 m to 2300 m but almost exclusively associated with basalt. Calcite is abundant at 916-920 m and 1096-1100 m in basaltic rock. Plagioclase altering to calcite is evidenced in at 1096 m (Figure 11) and calcite overprinting epidote is also seen at this depth.

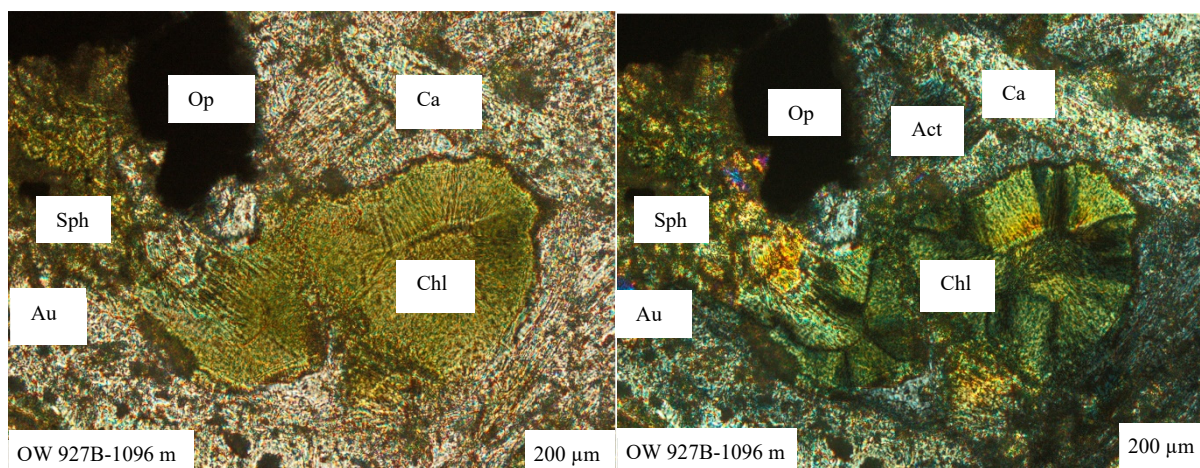


FIGURE 11: Photomicrograph of alteration minerals: Augite (Au), sphene (Sph), opaque mineral (OP), calcite (Ca), chlorite (Chl). a) Under plane polarized light; b) Crossed polarized light, alteration minerals replacing the primary minerals in basaltic rock.

*Pyrite* is shiny, brassy, sub-metallic, yellowish in colour with well formed cubic crystals. Pyrite is an opaque mineral and was therefore not specifically analysed during petrographic analysis. In cuttings analysis, pyrite occurs as precipitate in fractures, vesicles or in veins as well as dissemination sporadically from 280-1264 m. It disappears completely to the bottom of the well, but is abundant at 330-1026 m and to a lesser extent at 1144-1264 m. From 1264 m to the bottom of the well, it is absent.

*Fluorite*: In the sample cuttings, fluorite occurs as well-formed cubic crystals (octahedron) filling fractures, veins or vesicles but also occurring as relatively large primary crystals in rhyolitic tuff, which was seen at 736 m. Most fluorites observed were colourless in plane polarized light (ppl) and isotropic

in crossed polarized light (cpl) with perfect cleavage. It was observed in binocular analysis to be occasionally occurring at 334 m, 736 m, 1096 m, 1226 m, 1370 m, 1960 m and 2196 m depth. The fluorite in Olkaria geothermal field is associated with the movement of cool meteoric fluids rich in fluorine to deeper depths, where temperatures are greater than 100-150°C, depositing the fluorite (Leach and Muchemi, 1987). Fluorite is thought to be formed at temperatures between 130-150°C, but this has not been confirmed. Fluid inclusion analysis done on fluorite crystals indicates homogenization temperatures ranging between 80 and 280°C (Magotra et al., 2017).

*Secondary quartz* occurs as precipitations in lining of fractures or infilling vesicles, e.g. at 1370-1372 m depth. At 1960-1962 m depth, it is also seen as part of the mineral sequence chlorite → sphene → quartz → illite. Secondary quartz replaces primary minerals. The first appearance of secondary quartz was at 334 m and it is assumed to indicate temperatures of above 180°C.

*Wairakite* was only observed in petrographic analysis at 2192 m depth in a tuff, appearing grey in cpl with extinction of black to white and showing a characteristic cross hatched twinning (Figure 11). Its occurrence is in association with epidote, quartz, and adularia. Appearance of wairakite indicates temperatures above 200°C.

*Prehnite* is first observed at 1090 m depth, while it is predominant around 2192-2206 m. Prehnite is also observed near the well bottom at 2972 m in petrographic analysis. It is noted to occur in veins in affiliation with epidote, chlorite, wairakite and actinolite. It is recognised in thin sections by its shear 'bow-tie' structure, with good cleavage in one direction and strong interference colours. The appearance of prehnite indicates temperatures of 240°C and above.

*Sphene* is encountered from the shallow depth of 495 m to the bottom of the well. It occurs as a replacement of oxides. Sphene is tan brown to blue/brown or pearl grey and subhedral with a diamond shape when well formed and with a high relief.

*Epidote*: In well OW 927B traces of epidote appeared in binocular analysis at 770 m depth but well grown crystals of epidote were observed from 992 m, occurring sporadically to the bottom of the well. In petrographic analysis, epidote has high interference colours from yellow, yellowish green to yellowish pink in crossed polars. In plane polarized light, it is slightly pleochroic from colourless to yellow, green or yellowish green to green colour. Epidote is formed at a minimum temperature of 230°C (Reyes, 2000).

*Actinolite* is observed to occur occasionally from 1090 m to 2450 m depth. In binocular analysis, actinolite is green to grey green colour and coarse grained with fibrous, elongated laths like crystal aggregates. In thin sections, it is pale green to dark green and shows pronounced pleochroism with moderate relief. The interference colours are dominated by blue second order and green second order colours. Actinolite occurs as a replacement of pyroxene and oxides at 1096 m and 2450 m depth, respectively, and as precipitating in fracture veins at 2366 m depth forming a mineral sequence with epidote, clays and quartz. It occurs in association with epidote, garnets (Figure 12) and wollastonite. First appearance of actinolite at 1090 m depth indicates temperatures of minimum 280°C.

*Garnet* was identified in binoculars at 2134-2178 m depth where it appears cubic, deep red and occurs in clusters. In petrographic analysis, garnet is isotropic with no cleavage and has moderate relief. It occurs together with actinolite at 2182-2216 m depth (Figure 12). The presence of garnet normally indicates temperatures over 300°C (Bird et al., 1984).

*Adularia* occurs as a replacement of primary sanidine feldspar, as euhedral crystals lining fractures or cavities and can also be found infilling open space in the groundmass. It is often confused with sanidine, which is a primary mineral, and wairakite. In well OW 927B adularia was identified in thin sections at 1370-1372 m depth as replacement of feldspar and in association with chlorite (Figure 13). At 2192-2196 m depth, it occurs in a mineral sequence of wairakite → epidote → quartz → adularia.

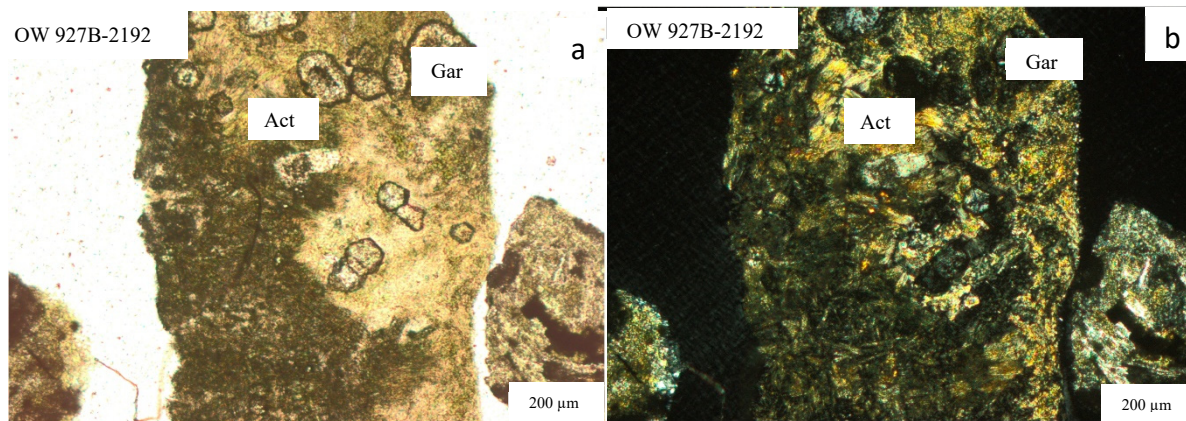


FIGURE 12: Actinolite (Act) and garnet (Gar) observed a) under plain polarized light and b) crossed plain polarized light

### 5.3 Mineral evolution and sequence of formation

During the history of a geothermal system, minerals are formed and their formation is controlled by their physiochemical properties. They are formed either by replacement of primary minerals or deposition depending on temperature. Hence, their depositional sequence can be used to explore the parent thermal history and the relative time scale of alteration minerals. Table 4 summarizes the mineralogy distribution and sequences within different lithologies from petrographic analysis of OW 927B. Temperature reversals/retrogrades were noted as, for example, calcite is seen overprinting epidote at 916 and 1096 m depth.

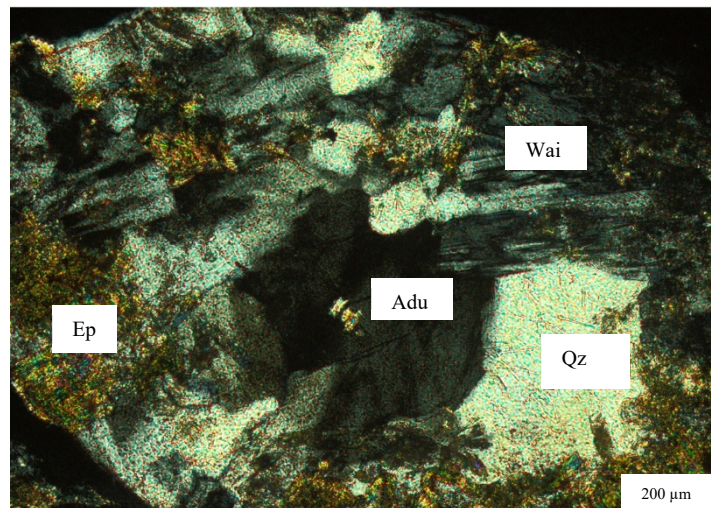


FIGURE 13: Photomicrographs showing adularia (Adu), wairakite (Wai), quartz (Oz) and epidote (Ep) observed under crossed polarized light at 2192 m tuff

### 5.4 Alteration mineral zonation

In OW 927B, the sequence of mineral assemblages relates to increased temperature and depth. Clay minerals are the most common alteration minerals. By using binocular, petrographic, XRD and electron microprobe analysis, five alteration zones have been identified in the well. The zones are identified by the first appearance of the succession clay minerals described in section 6.

*Unaltered zone (0-162):* The lithology in the zone comprises pyroclastics and a thin layer of rhyolite. Not much alteration is noted.

*Zeolite-illite zone (162-600):* Appearance of zeolites first noted at 162 m depth in the binocular microscope and at 492 m depth under petrographic microscope and traces of illite identified by XRD analysis at 334 m depth (Table 4). Other minerals noted are chalcedony, fluorite and well-formed pyrite cubes.

*Chlorite-illite zone (600-916):* The rock formation at this zone is noted to be moderately altered to green and brown clays. Chlorite and illite dominate this zone, as it is indicated by the XRD analysis (Table 4). Total loss of circulation is noted at this depth.

TABLE 4: Summary of mineralogy distribution and mineral sequences in well OW 927B identified in petrographic analysis

Depth (m)	Lithology	Primary minerals	Secondary minerals	Mineral sequence	Retro-grade/prograde	Remarks
334	Lithic tuff	Gl, qz,	Flt			Fresh rock with quartz
492	Rhyolite	Gl, qz, fel and plg	Py, cl, zeo, qz	Zeo→cl Qz→cl	Prograde	Slightly vesicular
736	Rhyolitic tuff	Gl fels, ox	Flt, qz, py, sph	Qz→cl	Prograde	Veining
916	Basalt	Px, olv, plg, ox	Chlo, ep, cal, sp qz, flt	Ep→cal Qz→cal	Retro-grade	Calcite abundant
1096	Basalt	Olv, plg, px, ox	Flt, chlo, sph, act, ep	Ep→cal	Retro-grade	High alteration
1226	Basalt	Olv, plg, px, ox	Flt, ep, cal, alb, act, sph	Cal→qz		Interstitial porosity
1370	Sedimentary tuff	Fels, qz	Flt, qz, adu, chlo, sph	Qz→cl		Medium alteration
1610	Trachyte	San	Qx, cl, flt	Flt→qz→cl	Prograde	Low alteration
1960	Trachyte	San, ox,	Flt, sp, qz, act, chlo, adu	Chlo→sp→qz→illite	Retro-grade	Poorly vesicular
2192	Tuff	Ox	Ep, pre, sph, alb, wai, chlo, adu, gar	Wai→ep→qz→adu	Retro-grade	Medium alteration
2450	Trachyte	Riebeckite, San, ox	Ep, qz, act, sph,	Qz→sph→ep	Prograde	
2972	Basalt	Px, plg, olv	Preh, qz, epidote			

**Abbreviation:** gl: glass, plg-fel: plagioclase-felspar, san: sanidine, px: pyroxene, olv: olivine, opa: opaque, cal: calcite, ox: oxides, chal: chalcedony, qz: secondary quartz, wai: wairakite, alb: albite, act: actinolite, pre: prehnite, ep: epidote, wol: wollastonite, zeo: zeolite, chlo: chlorite, cl: clay, flt: fluorite, sp: sphene, adu: adularia, gar: garnet, py: pyrite.

*Epidote-chlorite-illite zone (916-1090 m):* The appearance of crystalline epidote marks the upper boundary of this zone. The first occurrence of epidote was found in cuttings with binocular analysis at 916 m depth. It indicates an alteration temperature of more than 240°C.

*Actinolite-epidote-chlorite-illite zone (1090-2990):* The first appearance of actinolite was used to mark the upper boundary of this zone. It was first observed at 1096 m depth in thin sections and disappeared again between 1200-1600 m. It indicates an alteration temperature of 280°C and more.

## 5.5 Aquifers and feed zones

Sources of permeability in Olkaria Domes geothermal field include lithological contacts, fractures and faults or fragment contacts in breccia (Omenda, 1998). Within the well of study, permeability has been inferred from the loss of circulation fluid, intensity of alteration, lithological contacts like sedimentary tuff or breccia and temperature recovery logs. Permeable fissure channels are characterized by adularia occurring together with quartz and calcite (Steiner, 1968; Browne, 1970; Browne, 1978). Pyrite and calcite, which are indicators of permeability, were observed sporadically below 160 m depth and disappearing below 1250 m. The calcite occurs again in small amounts from 1900 m to 2300 m, but very minimal. An aquifer, which is cased off, is seen at 738-740 m, but at this depth there was total loss of circulation fluids during drilling.

At 1050-1120 m, a moderate feed zone is observed in the temperature profiles, but it is located in the upper sequence of Olkaria basalts. The feed zone is associated with cold inflow as oxidation increases, and presence of fluorite and hematite minerals is noted. At 2200-2250 m, a minor feed zone is noted which is associated with highly altered basaltic rock. A moderate feed zone is seen from temperature profiles in trachyte rock at 2460-2550 m, with an increase in temperature. Circulation of hotter fluids in the well at this depth is evidenced by the disappearance of oxidation, hematite and fluorite. Figure 14 illustrates the temperature profiles and feed zones observed in the well.

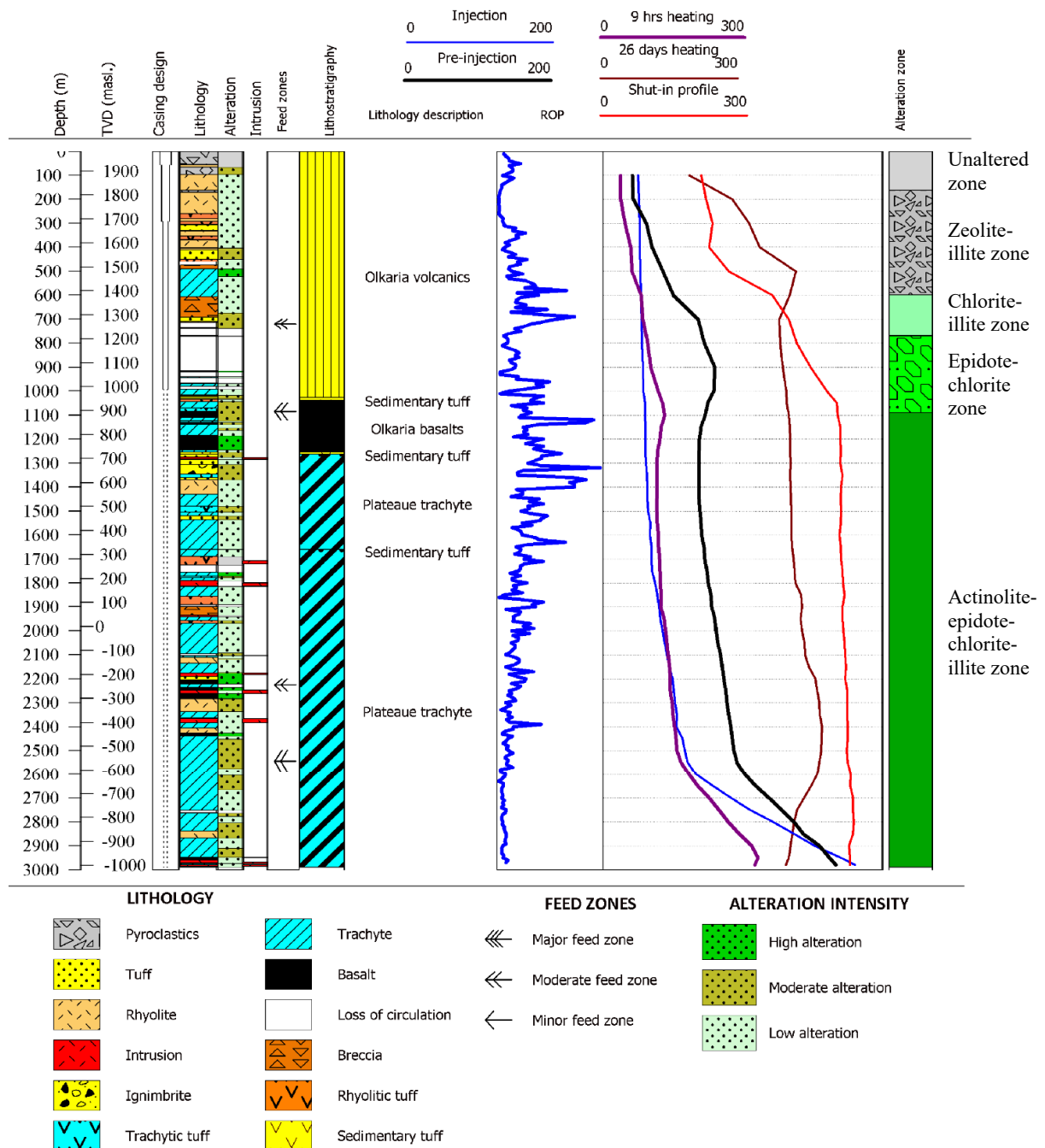


FIGURE 14: Lithology, lithostratigraphy, rate of penetration (ROP) and temperature profiles

## 6. DISTRIBUTION OF CLAY MINERALS WITHIN THE ROCK

Utada (1980) defined hydrothermal alteration as a rock alteration where the regional geothermal gradient in each area interacts with the surrounding rocks. The formation of clay involves weathering, diagenesis, and hydrothermal alteration. Hydrothermal alteration is controlled by solution composition, temperature, and pressure. In this study, we will focus on hydrothermal clay alteration in well OW 927B.

Normally, hydrothermal mineral precipitation occurs in the presence of a heat source, permeability (vesicles and/or rock fractures) and they are affected by the fluid composition, pressure, and time. The importance of clay minerals is evident in the characterization of hydrothermal alteration zones of active and fossil geothermal systems. The clay minerals encountered in OW 927B are listed below. Clay analysis and identification of minerals in the well was done using four different analyses. Firstly, using the binocular microscope for identification of rock type, the intensity of alteration and the type of alteration mineralogy, whether it is by precipitation or by replacement. Secondly, the petrographic microscope, which is used to confirm and further analyse, what was seen in the binocular microscope. Mineral sequences are better defined in thin sections and identification and classification of hydrothermal alteration minerals such as clays are easier to conduct (Figure 15). Thirdly, XRD analysis was used to quantify and confirm the type of clays occurring at each depth analysed. The final step involved using the electron microprobe analysis, which utilizes the X-rays of elements that are obtained in an energy dispersive spectrometer (EDS) to characterize the chemical composition of the clay and produce a backscattered image (Figure 15) together with compositional maps. Clay minerals were selected carefully under the petrographic analysis and in each thin section, 5 different points were

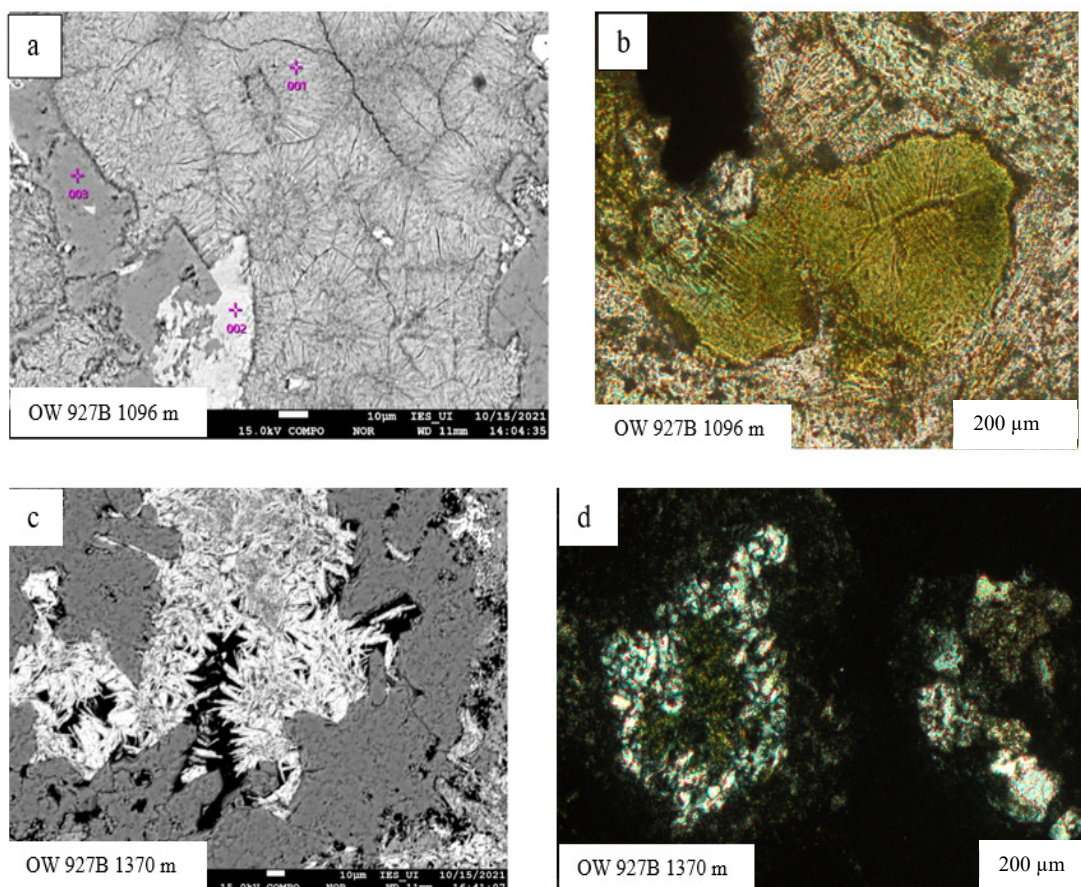


FIGURE 15: a) and c) backscattered electron images of chlorite at 1096 m and 1370 m depth from OW 927B. b) and d) photomicrographs of chlorite. The figures show chlorite both as a replacement of primary minerals (a, b) and filling vesicles (c, d).

selected and mapped for microprobe analysis. After the microprobe analysis the data was filtered by removing points where the chemical content of calcium and silica was very high. The structural formula was calculated in accordance with Deer et al. (1992) and those recalculations were based on 24 oxygens for illite and 36 oxygens for chlorite in the structure for the clays. Clay minerals contain water, but hydrogen is not easily detected with energy dispersive spectrometer (EDS) analysis. Furthermore, scanning electron microscopy and energy dispersive x-ray spectroscopy (SEM-EDS) analyses are not calibrated against a standard, thus the clay analyses with this method are semi-quantitative.

### 6.1 Distribution of clay minerals in the well

*Smectite*, which generally occurs in argillic alteration facies, is a product of hydrolysis reactions replacing glass, plagioclase, feldspar and normally forms at temperatures below 160°C (Fulignati, 2020). In OW 927B, smectite was not identified in the XRD analysis.

*Kaolinite* is the key mineral of the intermediate argillic alteration facies. Their presence in hydrothermal alteration indicates low temperature of <150-200°C (Fulignati, 2020). It was identified in the XRD analyses of sample cuttings at the depth of 334 m and 494 m with a peak of 7.1Å in both untreated, glycolated and heated samples.

*Chlorite* is a common mineral normally found in prophylic alteration and suggests temperature above 220°C (Fulignati, 2020). Chlorite mainly occurs in veins and vesicles or as a replacement of mafic minerals like pyroxene and olivine as well as glass. The XRD analyses indicates that chlorite is present from 736 m to 1370 m (Table 5). Chlorite at 916-920 m was identified in a thin section as an infilling in a vesicle. It was pale green in plain polarized light and appear dark green in crossed polarized light (Figure 16). At 1096-1100 m depth chlorite was identified in thin sections, XRD and microprobe analysis.

TABLE 5: XRD analysis of clay minerals in OW 927B

No	Depth (m)	d (001) Å untreated	d (001) Å glycolated	d (001) Å heated	d (002) Å untreated	Type of clay	Rock type
1	334	10.1	10.1	10.1	7.2	Traces of illite, kaolinite	Rhyolitic tuff
2	494				7.1 6.5	Kaolinite Plagioclase feldspars	Rhyolite
3	736	14.5 10.2	14.5 10.2	14.5 10.2		Chlorite Illite	Rhyolitic tuff
4	916	14.4 10.2	14.4 10.2	14.9 10.2	7.2	Chlorite Illite chorite	Basalt
5	1226	14.9 10.2	15.6 10.2	14.9 10.2	7.1 7.2	Mixed layer clay Illite, amphiboles	Trachyte
6	1370	14.4 15.6	14.4 15.6	14.4 15.6	8.6	Chlorite Actinolite/amph	Sedimentary tuff
7	1610	12.4 10.1 15.6	12.4 10.1 15.6	12.4 10.1 15.6	7.1	Fe-rich chlorite? Illite	Trachyte
8	1764	12.4 10.2	12.4 10.2	12.4 10.2	7.2 8.5 6.4	Fe-rich chlorite? Illite, Amphiboles Plagioclase feldspars	Trachyte
9	2192	10.1	10.1	10.1	6.8	Illite, plagioclase feldspar	Tuff
10	2450	10.1	10.1	10.1	8.5	Illite, amphiboles	Trachyte

*Illite*: In a hydrothermal environment, illite normally forms at temperature above 200-220°C up to about 350°C (Fulignati, 2020) as an alteration of K-feldspar and plagioclase. In OW 927B, illite was identified at 736 m depth by petrographic analysis. It is colourless in plain polarized light and shows fine shiny crystals in crossed polarized light. It was also identified in most of the XRD samples with peaks between 10-10.3 Å (Appendix II).

*Mixed layer clays (MLC)* are identified with XRD at 1226 m depth, with the untreated sample producing a peak of 14.9 Å. When glycolated, the peak shifts to 15.6Å, and when heated it collapses. The peaks for the illite/chlorite clay mixture are unchanged at 10.2 Å and 7.1 Å for all runs. The sample also contains amphiboles (actinolite) according to the peak at 8.5 Å in the XRD analysis (Appendix 2). MLC with smectite rarely occurs at greater depths due to an increase in temperature, but when it occurs, it may indicate possible cross flow in the well is observed, where cooler fluids may be involved. This could be the case of this well.

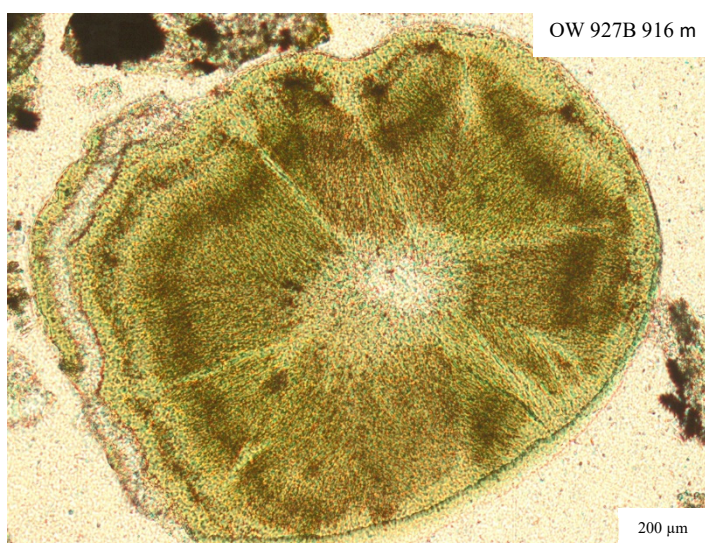


FIGURE 16: Photomicrograph of fibrous chlorite under plain polarized light at 916 m

## 6.2 Clay assemblage and composition in relation to rock type

Three different rock types were selected for SEM-EDS analysis for a first outline of potential compositional variation of clays dependent on rock type. Clays in basaltic lava at 1096 m depth, rhyolitic tuff at 2192 m and sedimentary tuff at 1370 m depth were selected for analysis.

### 6.2.1 Basaltic rock and clay hydrothermal alteration

At 918 m depth in basaltic rock, the XRD analysis on clay indicates the presence of illite with a 10.2 Å peak and chlorite with a d (001) 14.4 Å peaks in untreated and glycolated samples. When the sample is heated, the peak shifts to 14.9 Å. In the d (002) spacing at 7.1 Å, the untreated and glycolated peak has a high intensity, but when the sample is heated it appears shorter and seems to have shifted (unstable chlorite). The analysed basaltic rock contains both illite and chlorite clay. Based on semi-quantitative SEM-EDS analyses the chlorite exhibits variations in Fe composition of 33-39 wt%, while interlayered chlorite-illite clay has a relatively homogenous composition (Table 6).

### 6.2.2 Rhyolitic tuff in relation to clay alteration minerals

The chemical composition of clay minerals in rhyolitic tuff rock is shown in Table 7. Tuffs are generally easily altered to clay minerals. At 2192 m depth, the sample cutting analysis showed the presence of highly altered tuff rock. XRD analysis indicated the presence of illite clay and the peaks at d (001) showing 10.1 Å peak with higher intensity for the heated sample and shorter peak (smaller intensity) for the untreated and glycolated sample. SEM-EDS analyses indicate that illite clay is interlayered with chlorite in the rhyolitic tuff. The clays are richer in silica and potassium compared to the clays in basaltic rock, suggesting a higher proportion of illite in the interlayer illite-chlorite clays. Table 7 shows the chemical analyses of clays in rhyolitic tuff with 33-42 wt% of SiO<sub>2</sub>, 15-37 wt% of FeO<sub>tot</sub>, 5-21 wt% of MgO, 10-17 wt% of Al<sub>2</sub>O<sub>3</sub> and 4-10 wt% K<sub>2</sub>O.

TABLE 6: Representative SEM-EDS chemical analysis of interlayered illite-chlorite mixed layer clays and chlorite in basalt at 1096 m depth. Analyses are normalized to 100 wt%.

Point	Chlorite-illite		Chlorite			
	1	2	3	4	5	6
SiO <sub>2</sub>	37.49	36.93	34.86	33.15	31.4	31.78
TiO <sub>2</sub>	0	0	0	0	0	0
Al <sub>2</sub> O <sub>3</sub>	14.24	14.01	16.36	15.45	17.35	15.19
FeO <sub>tot</sub>	30.52	27.7	33.3	37.21	38.28	39.51
MgO	13.73	13.93	14.34	13.32	12.25	13.06
CaO	0	0	0.48	0.41	0.4	0.46
Na <sub>2</sub> O	0	0	0	0	0	0
MnO	0	0	0	0	0	0
K <sub>2</sub> O	4.02	3.45	0.66	0.48	0.31	0
Number of cations based on 24 oxygens			36 oxygens			
Si	6.05	6.12	5.62	5.47	7.83	7.98
Al	1.95	1.88	2.38	2.53	0.17	0.02
Al	0.76	0.86	0.73	0.48	4.93	4.47
Ti	0.00	0.00	0.00	0.00	0.00	0.00
Fe <sub>tot</sub>	2.75	2.56	2.99	3.43	5.32	5.53
Mg	3.30	3.44	3.45	3.28	4.55	4.89
Ca	0.00	0.00	0.08	0.07	0.11	0.12
Na	0.00	0.00	0.00	0.00	0.00	0.00
Mn	0.00	0.00	0.00	0.00	0.00	0.00
K	0.83	0.73	0.14	0.10	0.10	0.00

TABLE 7: SEM-EDS chemical analysis for interlayered illite-chlorite in rhyolitic tuff at 2192 m. Analyses are normalized to 100 wt%.

Point	1	2	3	4	5	6	7	8
SiO <sub>2</sub>	33.88	38.53	41.76	42.3	42.96	41.73	33.04	37.97
TiO <sub>2</sub>	0	0.54	0	0	0	0	0	0
Al <sub>2</sub> O <sub>3</sub>	14.43	13.37	11.12	10.46	11.07	12.59	17.05	13.06
Fe <sub>2</sub> O <sub>3</sub>								
FeO <sub>tot</sub>	37.21	31.25	21.77	18.46	17.57	15.13	33.17	24.75
MgO	8.53	8.65	14.9	16.07	16.48	21.26	12.97	12.68
CaO	0	0	0	0	0	0	0	0
Na <sub>2</sub> O	0	0	0	0	0	0	0	0
MnO	0	0	0	0	0	0	0	0
K <sub>2</sub> O	4.95	9.82	10.46	9.87	9.34	9.29	3.77	8.77
Number of cations based on 24 oxygens								
Si	5.80	6.30	6.67	6.82	6.84	6.38	5.44	6.32
Al(t)	2.20	1.70	1.33	1.18	1.16	1.62	2.56	1.68
Al	0.71	0.88	0.76	0.81	0.92	0.65	0.75	0.88
Ti	0.00	0.00	0.00	0.00	0.00	0.00	0.00	0.00
Fe <sub>tot</sub>	3.55	2.85	1.94	1.66	1.56	3.45	3.05	2.30
Mg	2.18	2.11	3.55	3.86	3.91	3.48	3.18	3.15
Ca	0.00	0.00	0.00	0.00	0.00	0.00	0.00	0.00
Na	0.00	0.00	0.00	0.00	0.00	0.00	0.00	0.00
Mn	0.00	0.00	0.00	0.00	0.00	0.00	0.00	0.00
K	1.08	2.05	2.13	2.03	1.90	1.81	0.79	1.86

### 6.2.3 Sedimentary tuff in relation to clay alteration

Sedimentary tuff in the well is highly oxidized and highly altered. At 1370 m, XRD and microprobe (SEM-EDS) analysis were done to determine the clay type. Chlorite infillings in a vesicle were identified using petrographic analysis (Figure 15). XRD analysis showed peaks of similar characteristics as chlorite in the basalt, but for d (001) spacing the untreated and glycolated peaks were at 14.4 Å and the heated sample showed a little shift. The d (002) spacing of chlorite showed high peaks of untreated and glycolated samples at 7.1 Å, while the heated peak was much shorter (Appendix 2). The chemical analysis indicates that the clay consists of iron-rich chlorite with lower silica content (Table 8) compared to the basaltic rock and rhyolitic tuff. The FeO rich chlorite clays is likely a result of high temperature hydrothermal fluids interacting with the rock and high oxidation and enrichment.

TABLE 8: Representative SEM-EDS chemical analysis of iron-rich chlorite in sedimentary tuff at 1370 m. Analyses are normalized to 100 wt%.

Analyses of iron-rich chlorite in sedimentary tuff at 1370 m									
Point	1	2	3	4	5	6	7	8	9
SiO <sub>2</sub>	24.81	24.85	25.41	24.83	25.58	25.4	24.9	24.43	25.49
TiO <sub>2</sub>	0	0	0	0	0	0	0	0	0
Al <sub>2</sub> O <sub>3</sub>	20.01	18.43	19.55	19.57	18.51	18.22	20.1	19.6	18.18
FeO <sub>tot</sub>	55.18	53.61	51.52	55.6	51.79	51.22	55	55.97	52.47
MgO	0	1.92	1.76	0	0.87	1.58	0	0	1.65
CaO	0	0	0	0	0	0	0	0	0
Na <sub>2</sub> O	0	0	0	0	0	0	0	0	0
MnO	0	1.69	1.26	0	3.25	3.58	0	0	1.48
K <sub>2</sub> O	0	0	0	0	0	0	0	0	0
Number of cations based on 36 oxygens									
Si	6.81	6.81	6.92	6.84	7.02	6.97	6.83	6.75	7.02
Al	1.19	1.19	1.08	1.16	0.98	1.03	1.17	1.25	0.98
Al	5.28	4.76	5.20	5.19	5.00	4.86	5.32	5.13	4.92
Ti	0.00	0.00	0.00	0.00	0.00	0.00	0.00	0.00	0.00
Fe <sub>tot</sub>	8.45	8.19	7.82	8.53	7.92	7.83	8.41	8.62	8.06
Mg	0.00	0.78	0.71	0.00	0.36	0.65	0.00	0.00	0.68
Ca	0.00	0.00	0.00	0.00	0.00	0.00	0.00	0.00	0.00
Na	0.00	0.00	0.00	0.00	0.00	0.00	0.00	0.00	0.00
Mn	0.00	0.39	0.29	0.00	0.76	0.83	0.00	0.00	0.35
K	0.00	0.00	0.00	0.00	0.00	0.00	0.00	0.00	0.00

### 6.3 Ternary diagrams

The composition of clays in the basalt, rhyolitic tuff and sedimentary tuffs is plotted in two ternary diagrams (Figure 17). The ternary diagram for Al<sub>2</sub>O<sub>3</sub>-FeO-MgO shows that the Fe and Al in clays in basalt and the rhyolitic tuff are half of the composition; the clay in the sedimentary tuff is more Fe rich. The K<sub>2</sub>O-FeO-MgO ternary diagram confirm that clays in the sedimentary tuff are Fe rich and poor in K and Mg. Clays in the rhyolitic tuff are more K-rich than the clays in the basaltic rock and a portion of the basalt clays have more Fe and only minor amounts of Al.

Based on SEM-EDS analyses of clays in basalt, there are two types of clays: chlorite and interlayered chlorite-illite clays. The rhyolitic tuff contains interlayered illite-chlorite clay with higher proportion of illite clay and thus higher K<sub>2</sub>O concentration compared to the interlayered chlorite-illite clays in basalt. The sedimentary tuff contains Fe-rich chlorite with 51-55 wt% of Fe and the XRD analysis at 1370 m indicates that chlorite clay is dominant at this depth.

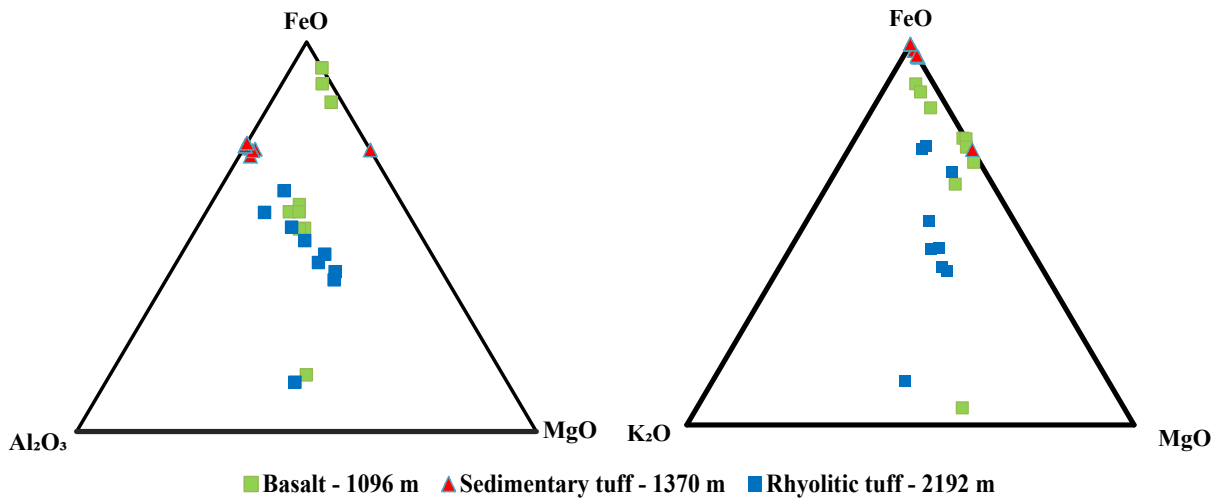


FIGURE 17: Ternary diagram of clay minerals composition of basalt, rhyolitic tuff, and sedimentary tuff

7. DISCUSSION

7.1 Geological, temperature profile and geophysical interpretation

The lithology of OW 927B was interpreted by using binocular and petrographic microscopes. The pyroclastic and rhyolite at the top correspond to Olkaria commendites. The trachyte, breccia, and rhyolitic tuff correspond to upper Olkaria volcanics. The Olkaria basalt is represented by basalt with intercalation of trachyte and rhyolitic tuff. The plateau trachytes dominate at depth and form the reservoir formation. It is also noted that the cap rock basalt occurs at greater depth compared to other wells in this area. However, as there was loss of circulation between 730-910 m depth, it is difficult to identify the exact depth of the upper limit of the basalt and it may be shallower than 1000 m, which have been defined here (Figure 18). For OW 927B basalt, the cap rock, is observed at 1086 to 1250 m. This is much deeper when compared to 400 m to 600 m in other productive wells. In OW 914, basalt was noted at 480 m, while in OW 916 at 454 m and in OW 911A at 722 m.

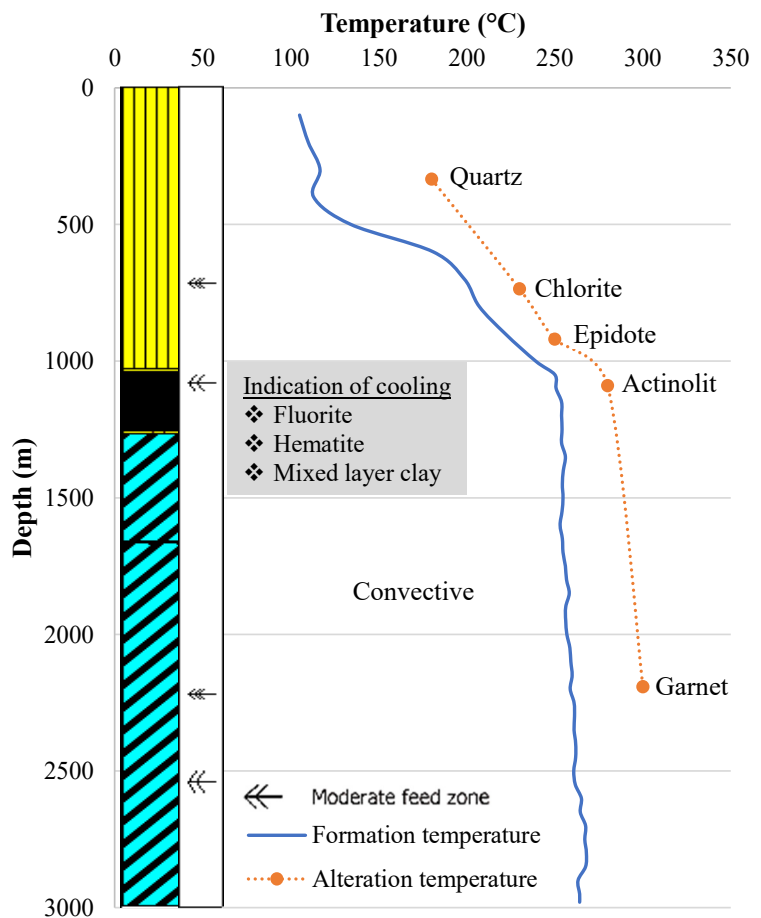


FIGURE 18: Formation and alteration temperature for OW

The formation temperature (Figure 18) increases steadily down to 1050 m and then remains almost constant indicating a convective system to the bottom of the well. Comparison with the alteration temperature suggests that the well has experienced at least 20-40°C cooling since the height of alteration. The presence of fluorite and hematite (unstable) at deeper depths in the well indicates conditions of cooling. The conditions controlling cooling in the well can be associated with the processes of forming these minerals. Starting at 1100 m depth, the oxidation and hematite (unstable) tend to increase down to 1800 m. Oxidation occurs in environments where oxygen is available. Abundance of oxidation and hematite at this depth could indicate movement of cold meteoric fluids. The fluorite in Olkaria geothermal field is associated with the movement of cool fluids rich in fluorine to greater depths where temperatures are greater than 100-150°C, causing deposition of the fluorite (Leach and Muchemi, 1987). Thus, indications of cold inflow into the well and the movement of cold fluid and deposition of fluorite minerals.

According to Lagat (2004), the thermal gradient at depth decreases slightly to the southeast towards well OW 903, and sharply to the southwest towards well OW 902, which is cold and probably extending towards OW 927B and OW 911. The drop in both pressure and temperature profiles from well OW 901 to wells OW 902, OW 927B and OW 911 suggests they are located in an outflow zone.

## 7.2 Clay alteration minerals in relation to temperature

Clay plays a big role in determining the temperature distribution in geothermal fields and assists in reservoir hydrological modelling. Clay minerals adopt quickly to new thermal conditions and are often used to map the thermal fluctuations of the geothermal system. Common and useful clay minerals for mapping of fluctuations are smectite, mixed layer clay, illite, and chlorite. If the formation temperature, which is the current temperature, is lower than the alteration temperature in the well, this suggests that the well has cooled with time. Fluorite, hematite (unstable) and mixed layer clay is seen occurring and overprinting high temperature minerals like epidote, actinolite and adularia at 736 m to 1960 m. This could suggest cold inflow of fluids into the well. Illite occurs in the well from a shallow depth of 334 m all the way to the bottom of the well. Occurrence of illite indicates that the geothermal reservoir has temperatures that have exceeded 200°C. Chlorite is another common clay mineral, which is used as a temperature indicator. It occurs in association with epidote, illite, actinolite, and calcite. The appearance of chlorite indicates reservoir temperatures of at least 220°C.

Clay minerals have been used as makers of paleo-conditions in both fossil and active geothermal systems. They have been proven useful in estimating temperature based on modification of the crystal structure of the mineral (Lagat, 2004). The changes in the well are observed from kaolinite, mixed layer clay, illite and chlorite at the bottom of the well. Four hydrothermal alteration zones are recognised in the well caused by increasing temperature and depth which include a) the zeolite-illite zone, b) illite chlorite zone, c) epidote-illite-chlorite zone, and d) actinolite-epidote-illite-chlorite zone.

## 7.3 Clay minerals in relation to rock types

Clay minerals give intrinsically broad peak lines because of small scattering domains, structural disorder, mixed layering or a combination of these factors. Poor crystallinity due to defects between unit cells or small crystal size causes changes in peak height but not integrated intensity. Chlorites are rich in either Al, Fe or Mg. If the crystallites absorb more than 1% of the incident energy, the peak intensities change. Fe-rich chlorites are heavy, which is why the peaks in sedimentary tuffs and some of the basalts are high. Two common ions exert important controls in chemical composition and crystal structure of clay minerals: The Fe in chlorite at the octahedral site and the K in illite interlayer. The chlorites in the sedimentary tuff contain more than normal amounts of iron and are expected to have a low content of H<sub>2</sub>O. The high content of Fe is probably caused by high oxidation of the rock. The basalt and the rhyolitic tuff in the series FeO-MgO-Al<sub>2</sub>O<sub>3</sub> contain relatively high amounts of Al

compared to Mg. When we have aluminium rich chlorite it is stable below 370-390°C; at higher temperature it is decomposed to magnesian chlorite (Deer et al., 1992).

The SEM-EDS analysis reveals the compositional variation of clays and clay assemblages in relation to the rock type. The analysis supports the XRD analysis in outlining compositional variations. Further analysis can improve the accuracy of the XRD analysis as well as the understanding of the sensitivity of clay composition relative to rock composition and fluid rock interaction.

## 8. CONCLUSION

The lithostratigraphy of well OW 927B consists of Olkaria volcanics (pyroclastics and comendites) (0-1026 m), Olkaria basalts (1020-1254 m), and Plateau trachytes (1254-2990 m), with major loss of circulation at 730-910 m.

The current measured formation temperature is lower than the alteration temperature, indicating cooling in the well. The occurrence of hematite (unstable), mixed layer clay and fluorite minerals in the reservoir also suggest cooling of the system in the vicinity of the well.

A few minor feed zones at 1050-1120 m and 2200-2250 m were identified in the well, with the main feed zone at 2460-2550 m depth. The analysis of the well shows that OW 927B has low permeability. The sources of permeability in the well include fractures, lithology contacts and lost zones.

The occurrence of basalts as the cap rock is at greater depth than in other wells in the area. The scarce occurrence of intrusions and the comparison of the formation temperature with the alteration temperature could indicate that OW 927B is located in an outflow zone or at the boundary of the Olkaria Domes geothermal system.

The chlorite and illite show systematic variations in chemical composition in relation to rock type and formation temperature, thus, allowing for the development of clay minerals as geothermometers.

The transition between two end-member clays involves changes in chemical composition that depend on the temperature, primary mineral of the rock type and the fluid interaction.

The clay composition was different in the three analysed rocks: Basalt contains chlorite and interlayered chlorite-illite clay, rhyolitic tuff contains interlayered illite-chlorite clay, and sedimentary tuff contains Fe-rich chlorite.

Further studies are needed to distinguish the chemical composition of the clay minerals, which occur as monomineralic deposits, and more exploration work is needed in the area.

## ACKNOWLEDGEMENTS

I would like to take this chance to thank the Government of Iceland and GRÓ GTP for awarding me the fellowship, and my employer Kenya Electricity Generating Company PLC for granting me the six-months study leave. Special gratitude goes to the GRÓ GTP staff, Mr. Gudni Axelsson, Mr. Ingimar G. Haraldsson, Mrs. Málfríður Ómarsdóttir, Dr. Vigdís Hardardóttir, not forgetting former employer Mr. Markús A.G. Wilde.

I owe my gratitude to my supervisors Ms. Anette K. Mortensen and Mrs. Helga Margrét Helgadóttir for their dedication, guidance and technical support throughout the project, not forgetting Mr. Sigurdur Sveinn Jónsson for his assistance in XRD preparation, analysis and interpretation, Mrs. Anett Blischke

and Dr. Hjalti Franzson for the geological field trips and all ÍSOR staff for their lectures and contributions, which made the six-months training a success. I appreciate my fellow geologists and GRÓ GTP fellows 2021 for their support and assistance during my stay in Iceland.

Special thanks go to my husband Dr. Stephen Okoth and my daughters Jebet, Akinyi and Adhiambo, for your encouragement and persevering my absence during my six-month period, also to my house manager Lydia for taking care of my kids.

Finally, thanks to the almighty God for the protection and guidance.

## REFERENCES

- Ambusso, W.J., and Ouma, P.A., 1991: Thermodynamic and permeability structure of Olkaria north-east geothermal field: Olkaria fault. *Geothermal Resources Council Transactions*, 15, 237-242.
- Baker, B.H., 1986: Tectonics and volcanism of the southern Kenya rift valley and its influence on sedimentation in the African rifts. In: Frostick, L.E., Renaut, R.W., Reid, I., and Tiercelin, J.J. (eds.), *Sedimentation in the African Rifts*, Geol. Soc. Lond. Spec. Publ., 25, 45-57.
- Baker, B. H., and Wohlenberg, J., 1971: Structure and evolution of the Kenya rift valley. *Nature*, 229, 538-542.
- Bird, D.K., Schiffman, P., Elders, W.A., Williams, A.E., and McDowell, S.D., 1984: Calc-silicate mineralization in active geothermal systems. *Economic geology*, 79, 671-695.
- Bird, D.K., and Spieler, A.R., 2004: Epidote in geothermal systems. *Reviews in Mineralogy and Geochemistry*, 56, 235-300.
- Browne, P.R.L., 1970: Hydrothermal alteration as an aid in investigating geothermal fields. *Geothermics*, 2, 564-570.
- Browne, P.R.L., 1978: Hydrothermal alteration in active geothermal fields. *Annual Reviews of Earth and Planetary Science*, 6, 229-250.
- Browne, P.R.L., 1982: Mapping of geothermal discharge features. In: Hochstein, M.P. (ed.), *Introduction to geothermal prospecting*. Univ. of Auckland Publ., 67-69.
- Castaing, R., 1951: *Application of electron probes to local chemical and crystallographic analysis*. University of Paris, PhD Thesis, 166 pp.
- Clarke, M.C.G., Woodhall, D.G., Allen, D., and Darling G., 1990: *Geological, volcanological and hydrogeological controls on the occurrence of geothermal activity in the area surrounding Lake Naivasha, Kenya, with coloured 1:100 000 geological maps*. Ministry of Energy, Nairobi, 138 pp.
- Deer, W.A., Howie, R.A., and Zussman, J., 1992: *An introduction to the rock-forming mineral*. British library cataloguing in publication data, London, 696 pp.
- Elders, W.A., 1977: Petrology as a practical tool in geothermal studies. *Geothermal Resources Council Transactions*, 1, 85-87.
- Fulignati, P., 2020: Clay minerals in hydrothermal systems. *Minerals*, 10(10), 17 pp.

Haukwa, C.B., 1984: *Recent measurements within Olkaria East and West fields*. Kenya Power Co., internal report, 13 pp.

KenGen, 2012: *Stratigraphy and hydrothermal alteration mineralogy of well OW-915B*. Kenya Electricity Generating Company, internal report (unpublished), 40 pp.

Lagat, J.K., 2004: *Geology, hydrothermal alteration and fluid inclusion studies of the Olkaria Domes geothermal field, Kenya*. University of Iceland, Reykjavik, Iceland, MSc thesis, UNU-GTP, report 1, 79 pp.

Leach, T.M., and Muchemi G.G., 1987: Geology and hydrothermal alteration of the north and west exploration wells in the Olkaria geothermal field, Kenya. *Proceedings of the 9<sup>th</sup> New Zealand Geothermal Workshop, Geothermal Institute, Auckland*, 187-192.

Macdonald, R., Davies, G.R., Bliss, C.M., Leat, P.T., Bailey, D.K., and Smith, R.L., 1987: Geochemistry of high silica peralkaline rhyolites, Naivasha, Kenya rift valley. *Journal of Petrology*, 28, 979-1008.

Magotra, R., Nanga, S., Singh, P., Arora, N., and Srivastava, P., 2017: A new classification scheme of fluorite deposits. *International Journal of Geosciences*, 8, 599-610.

Meunier, A., 2005: *Clays*. Springer, Berlin Heidelberg New York, 472 pp.

Mungania, J., 1992: *Geology of the Olkaria geothermal complex*. Kenya Power Company Ltd., internal report, 38 pp.

Musonye, X.S., 2012: Borehole geology and alteration mineralogy of well OW-914A, Domes area, Olkaria geothermal field, central Kenya rift. Report 23 in: *Geothermal Training in Iceland 2012*. UNU-GTP, Iceland, 501-540.

Naylor, W.I., 1972: *Geology of the Eburru and Olkaria prospects*. United Nations Geothermal Exploration Project, report, 104 pp.

Omenda, P.A., 1998: The geology and structural controls of the Olkaria geothermal system, Kenya. *Geothermics*, 27(1), 55-74.

Omenda, P.A. (ed.), 2000: *Ranking of the geothermal prospects in the Kenya Rift Valley*. Contributions from: Lagat, J., Mungania, J., Mariita, N., Onacha, S., Simiyu, S., Opondo, K., Kubo, B.P., Ouma, P., Wetangula, G., and Kollikho, P., Kenya Electricity Generating Company, Kenya, internal report, 121 pp.

Okoo, J.A., 2013: Borehole geology and hydrothermal mineralisation of well OW-39A, Olkaria East geothermal field, Naivasha, Kenya. Report 24 in: *Geothermal Training in Iceland 2013*. UNU-GTP, Iceland, 547-574.

Otieno, V.O, and Kubai, R., 2013: Borehole geology and hydrothermal mineralisation of well OW-37A, Olkaria East geothermal field, Kenya. Report 2 in: *Geothermal Training in Iceland 2013*. UNU-GTP, Iceland, 105 pp.

Otieno, V., Okoo, J., Munyiri, S., Wanjohi, D., and Wanjohi A., 2014: *Structural mapping of Olkaria Southwest field, Olkaria geothermal project*. Kenya Electricity Generating Company, Kenya, internal report, 41 pp.

- Otieno, V.O., 2016: *Borehole geology and sub-surface petrochemistry of the Domes area, Olkaria geothermal field, Kenya, in relation to well OW-922*. University of Iceland, M.Sc. thesis, UNU-GTP, report 2, 95 pp.
- Reyes, A.G., 1990: Petrology of Philippine geothermal systems and the application of alteration mineralogy to their assessment. *J. Volc. Geoth. Res.*, 43, 279-309.
- Reyes, A.G., 2000: *Petrology and mineral alteration in hydrothermal systems: from diagenesis to volcanic catastrophes*. UNU-GTP, Iceland, report 18, 1998, 77 pp.
- Ronoh, I.J., 2012: Borehole geology and hydrothermal alteration of well OW-912B, Olkaria geothermal field, Kenya. Report 29 in: *Geothermal Training in Iceland 2012*, UNU-GTP, Iceland, 695-732.
- Simiyu, S.M., 2010: Status of geothermal exploration in Kenya and future for its development. *Proceedings of the World Geothermal Congress 2010, Bali, Indonesia*, 11 pp.
- Simmons, S.F., and Christenson, B.W., 1994: Origin of calcite in a boiling geothermal system. *Am. Jour. Sci.*, 294, 361-400.
- Smith, M., and Mosley, P., 1993: Crustal heterogeneity and basement influence on the development of the Kenya Rift, East Africa. *Tectonics*, 12, 591-606.
- Steiner, A., 1968: Clay minerals in hydrothermally altered rocks at Wairakei, New Zealand. *Clays and Clay Minerals*, 16, 193-213.
- Thompson, A.O., and Dodson, R.G., 1963: *Geology of the Naivasha area*. Government of Kenya Geological Survey, report 55, 80 pp.
- Utada, M., 1980: Hydrothermal alteration related to igneous acidity in Cretaceous and Neogene formations of Japan. *Mining Geol Jpn Spec issues*, 8, 67-83.

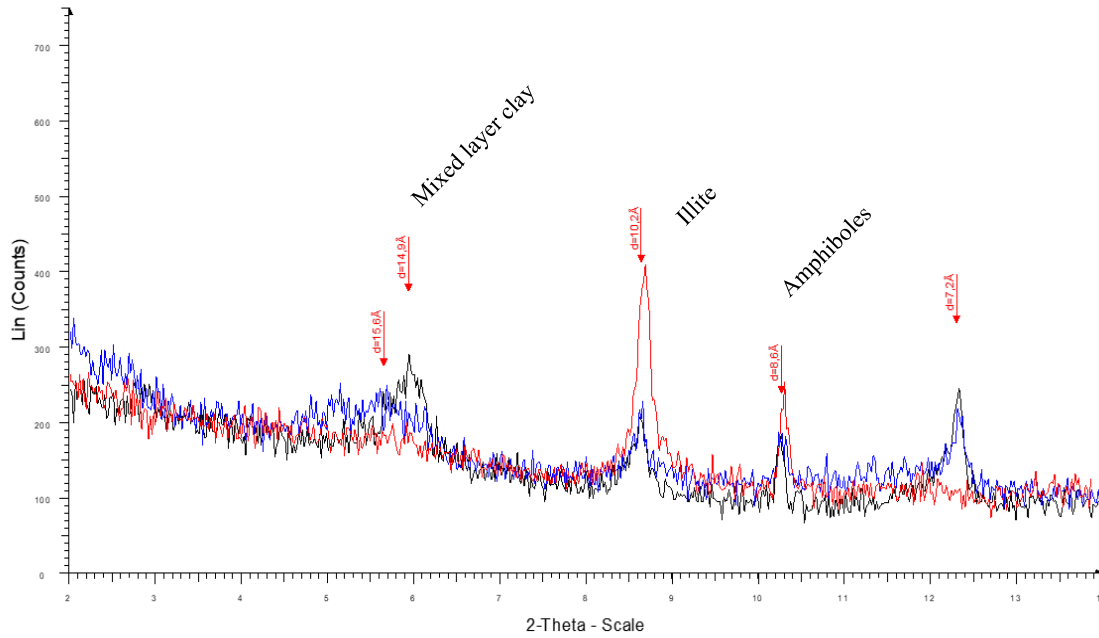
#### APPENDIX I: Clay analysis preparation

After careful washing of each sample in distilled water, about 2 g are put in a glass test-tube, the tube nearly filled with distilled water and put in a mechanical shaker. The sample is shaken for about four hours. The suspended clay-slurry is left to settle for about 10 minutes and then transferred onto a glass-slide using a pipette. The sample is left to dry in ambient temperature and humidity. The sample is measured after complete drying (UNT, untreated) and after measurement the sample is placed inside a closed desiccator above a container filled with ethylene-glycol. The sample is left in the ethylene-glycol fume for 24 hours and then measured (GLY, glycolated). Finally, the sample is heated in a furnace for about 1 hour in 550°C and after cooling, measured again (HIT, heated). The set of three measurements is then viewed superimposed using special software for X-ray diffraction data display (Bruker, Diffrac.Eva).

Each sample is measured from  $2\Phi = 2^\circ - 14^\circ$  in  $0.02^\circ$  increments (steps) and measured for 1 second in each step. The set-up is saved in a parameter file leir-a.dql. Each measurement takes about 20 minutes. The X-ray beam is confined using  $0.5^\circ$  divergence and receiving slits. The equipment used is a Bruker AXS D8 Focus, producing Cu  $k\alpha$  radiation with 1.54 Å wavelength at 40 kV and 40 mA. The detector used is a NaI scintillation counter.

APPENDIX II: Diffractograms from XRD clay analyses

OW-927B 1226-1230 m - Trachyte

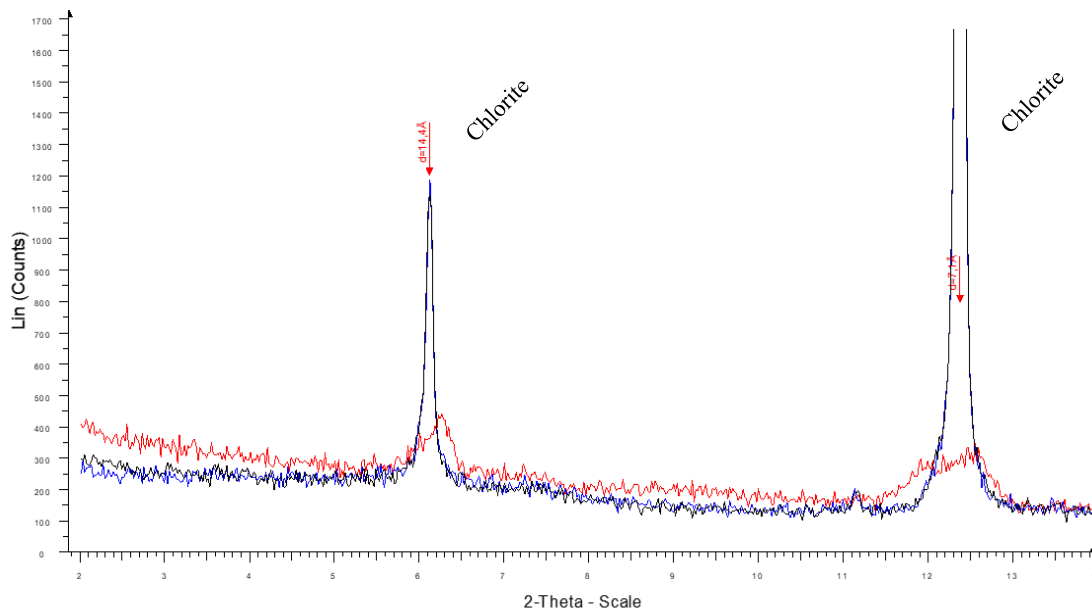


62262/C-5 UNT - File: 62262.raw - Type: 2Th/Th locked - Start: 2.000 ° - End: 14.000 ° - Step: 0.020 ° - Step time: 1. s - Temp.: 25 °C (Room) - Time Started: 5 s - 2-Theta: 2.000 ° - Theta: 1.000 ° - Chi: 0.00 ° - Phi: 0.00 °

62291/C-5 HIT - File: 62291.raw - Type: 2Th/Th locked - Start: 1.869 ° - End: 13.870 ° - Step: 0.020 ° - Step time: 1. s - Temp.: 25 °C (Room) - Time Started: 6 s - 2-Theta: 1.869 ° - Theta: 1.000 ° - Chi: 0.00 ° - Phi: 0.00 °

62320/C-5 GLY - File: 62320.raw - Type: 2Th/Th locked - Start: 2.000 ° - End: 14.000 ° - Step: 0.020 ° - Step time: 1. s - Temp.: 25 °C (Room) - Time Started: 6 s - 2-Theta: 2.000 ° - Theta: 1.000 ° - Chi: 0.00 ° - Phi: 0.00 °

OW-927B 1370-1372 - Sedimentary tuff



62263/C-6 UNT - File: 62263.raw - Type: 2Th/Th locked - Start: 2.000 ° - End: 14.000 ° - Step: 0.020 ° - Step time: 1. s - Temp.: 25 °C (Room) - Time Started: 5 s - 2-Theta: 2.000 ° - Theta: 1.000 ° - Chi: 0.00 ° - Phi: 0.00 °

62292/C-6 HIT - File: 62292.raw - Type: 2Th/Th locked - Start: 2.000 ° - End: 14.000 ° - Step: 0.020 ° - Step time: 1. s - Temp.: 25 °C (Room) - Time Started: 5 s - 2-Theta: 2.000 ° - Theta: 1.000 ° - Chi: 0.00 ° - Phi: 0.00 °

62321/C-6 GLY - File: 62321.raw - Type: 2Th/Th locked - Start: 2.000 ° - End: 14.000 ° - Step: 0.020 ° - Step time: 1. s - Temp.: 25 °C (Room) - Time Started: 6 s - 2-Theta: 2.000 ° - Theta: 1.000 ° - Chi: 0.00 ° - Phi: 0.00 °

OW-927B 1764-1766 m

